Ali Reza Ashrafi
Franco Cataldo
Ali Iranmanesh
Ottorino Ori *Editors*

Topological Modelling of Nanostructures and Extended Systems

Springer

Topological Modelling of Nanostructures and Extended Systems

CARBON MATERIALS: CHEMISTRY AND PHYSICS

A comprehensive book series which encompasses the complete coverage of carbon materials and carbon-rich molecules from elemental carbon dust in the interstellar medium, to the most specialized industrial applications of the elemental carbon and derivatives. A great emphasis is placed on the most advanced and promising applications ranging from electronics to medicinal chemistry. The aim is to offer the reader a book series which not only consists of self-sufficient reference works, but one which stimulates further research and enthusiasm.

Series Editors

Dr. Prof. Franco Cataldo
Via Casilina 1626/A,
00133 Rome, Italy

Professor Paolo Milani
Department of Physics
University of Milan
Via Celoria, 26
20133, Milan, Italy

VOLUME 7:
TOPOLOGICAL MODELLING OF NANOSTRUCTURES AND EXTENDED SYSTEMS

Volume Editors

Prof. Dr. Ali Reza Ashrafi
Department of Mathematics
University of Kashan
87317-5116, Kashan, Iran

Prof. Dr. Franco Cataldo
Department of Materials Science
Tor Vergata University
Rome, Italy

Prof. Dr. Ali Iranmanesh
Department of Mathematics
Tarbiat Modares University
Tehran, Iran

Prof. Dr. Ottorino Ori
Actinium Chemical Research
Rome, Italy

For further volumes:
http://www.springer.com/series/7825

Ali Reza Ashrafi • Franco Cataldo • Ali Iranmanesh
Ottorino Ori

Editors

Topological Modelling of Nanostructures and Extended Systems

Springer

Editors
Ali Reza Ashrafi
Department of Mathematics
University of Kashan
Kashan, Iran

Ali Iranmanesh
Department of Mathematics
Tarbiat Modares University
Tehran, Iran

Franco Cataldo
Department of Materials Science
Tor Vergata University
Rome, Italy

Ottorino Ori
Actinium Chemical Research
Rome, Italy

Dedicato al Prof. Ante Graovac,
amico e maestro per molti di noi.
Ciao TONKO !

Dedicated to Prof. Ante Graovac,
a teacher and a friend.
Bye TONKO!

Foreword

Among the chemical elements that populate the periodic table, carbon has arguably had the most dramatic impact in human civilization. Carbon appears naturally in two different crystalline forms known as diamond and graphite. The main difference among these two allotropes is given by the way in which carbon atoms are *connected* to each other. In graphite, carbon atoms form regular hexagonal lattices in which every atom is *connected* to three others. In diamond, however, carbon atoms are arranged into a variation of the face-centred cubic shape in which every atom is connected to the other four. This mere *connectivity* of the atoms defines a series of properties which remain invariant after any deformation of the molecule that does not involve breaking (or creating) any bond. When these topological arrangements of atoms are embedded into the three-dimensional (3D) space, other characteristic properties of the allotropes emerge. The cubic network of diamond, for instance, results in a very rigid structure which is characteristic of its hardness, while graphite forms the typical planar sheets that can displace one over the other. The first group of properties is referred to as *topological*, while the second group is referred to as *geometric*.

The mathematical differences between the topological and the geometric views of the molecular structure can be even more appreciated in another carbon allotrope: fullerenes.

The topology of fullerenes consists of carbon atoms which are connected to other three atoms; however, whereas graphite has only hexagons in their structure, fullerenes have also pentagons. Topologically speaking, fullerenes are planar like graphite, i.e. they can be embedded into a plane without their bonds being crossed. However, when fullerenes are embedded into the 3D space, their typical spherical shape emerges. This is a consequence of other physical and chemical properties of carbon atoms, such as hybridization. In fullerenes, carbon has sp_2 hybridization which, together with the appropriate location of the pentagonal rings, makes the spherical shape emerging.

From a chemist viewpoint, *topology* implies a series of physical and chemical properties such as hybridization and inter-atomic repulsion. which allow a better understanding of the properties of materials. For instance, in carbon nanotubes, the

different topological arrangements, i.e. armchair, zigzag or chiral, largely influence the electronic band structure of these molecules and their physical properties like the metallic or semiconducting character.

Carbon is so rich in its molecular arrangements that we can study topology and geometry by using it as an example. For instance, graphene can be used to study Euclidean geometry due to its zero Gaussian curvature. Fullerenes, on the other hand, can be used to illustrate spherical or elliptical geometry where the Gaussian curvature is positive and the sum of angles of a triangle is larger than 180°. Even more, it has been proved that carbon nanomaterials in which the surface bends with negative curvature, like in hyperbolic spaces, are also possible. The 'schwarzites' belong to this category of compounds.

The topologies of many of carbon nanomaterials are also nontrivial. Apart from the fullerenes with *genus* equal to zero, like the sphere, toroidal graphite has also been found to be stable, matching the topology with genus equal to one, like a torus. More exotic structures have also been proposed which correspond to topologies with genus larger than 20 and even to spheres with more than 20 handles. This volume presents some of these exciting carbon geometries and topologies. Interesting properties of fullerenes, nanotubes, graphene, schwarzites and other nanomaterials are inferred here from the analysis of the connectivity patterns of these topological arrangements. More sophisticated techniques are also explored, although the authors have mainly focused on the connectivity patterns defining the nature of these molecules.

This book will appeal to mathematicians as well as chemists, physicists and material scientists. The former, particularly the ones interested in exploring carbon allotropes and the nanomaterials deriving from them, will find the book of great interest as it exemplifies some of the concepts they use in their everyday work and it challenges them with some of the problems of this area. The latter, particularly the ones studying carbon materials, will be attracted by the basic concepts of topology and geometry examined in the book. Not only they will develop a better understanding of molecular, physical and chemical properties of these nanomaterials, but they will also get introduced to new topological and geometrical worlds still unexplored.

Carbon will surely surprise us all.

Glasgow   Ernesto Estrada
18/04/2012

Preface

Topological Modelling of Nanostructures and Extended Systems gathers the contributions of renowned leading experts in this new branch of science that we could also name 'Mathematical Nanoscience' and that were presented at the MATH/CHEM/COMP Meeting held in Dubrovnik, Croatia, in 2010.

This volume completes and expands upon the previously published title *The Mathematics and Topology of Fullerenes* (Carbon Materials: Chemistry and Physics series, Vol. 4, Springer 2011) by gathering the latest research and advances in materials science at nanoscale. It introduces a new speculative area and novel concepts like *topochemical reactions* and *coloured reactive topological indices* which allow the reader to gain a better understanding of the physical–chemical behaviours of extended systems. Moreover, a charming new family of *space-filling fullerenic crystals* is here analysed for the first time.

Mathematical chemistry is an interdisciplinary area with not only numerous theoretical developments but also countless applications to practical problems. The basal influence exercised on chemical and physical properties by *long-range topological mechanisms* links the various topics covered in the book. Carbon nanostructures, made by three-linked nodes variously connected, appear in fact quite sensitive to topological effects.

Nanonetworks have a spanning dimensionality. In fact, they can assume every possible dimensionality, from 0D (finite fullerenes) to 1D (nanotubes or nanoribbons), 2D (graphenic layers), 3D (diamond or schwarzites) and even to fractal dimensionality (fractal schwarzites). Such a characteristic makes them the optimal subjects for topological investigations. Moreover, topological modelling methods can be relied on to support the accuracy of large-scale first principles calculations, as it is largely documented in the original theoretically and experimentally results examined in this book.

In a way, we would like to think that this volume confirms what Prof. Harold Kroto, 1996 Nobel Prize for Chemistry, wrote in the Foreword of our previous title: 'Beauty Is Inherently Part of the Human Being Actions'.

And this could not be more true when thinking of Prof. Ante Graovac, the mind behind this volume, who prematurely passed away leaving us all with an immense sense of void. Words fail us to express our gratitude for this great academic, both a mentor and a friend.

We are grateful to Springer for giving us the opportunity to publish this book and for their top-quality professional support.

Dubrovnik, Croatia   Ali Iranmanesh
                                                                        Ali Reza Ashrafi
                                                                        Franco Cataldo
                                                                        Ottorino Ori

Contents

Contributors

Andrés Ayuela Centro de Física de Materiales (CFM-MPC) CSIC-UPV/EHU, San Sebastián, Spain

Ali Reza Ashrafi Department of Mathematics, Faculty of Mathematics, Statistics and Computer Science, University of Kashan, Kashan, Islamic Republic of Iran

Vincenzo Barone Scuola Normale Superiore, Pisa, Italy

Giorgio Benedek Dipartimento di Scienza dei Materiali, Università di Milano-Bicocca, Milan, Italy

Donostia International Physics Center (DIPC), Donostia/San Sebastián, Spain

Marco Bernasconi Dipartimento di Scienza dei Materiali, Universitá di Milano-Bicocca, Milan, Italy

Donostia International Physics Center (DIPC), Donostia/San Sebastián, Spain

Franco Cataldo Actinium Chemical Research, Rome, Italy

Mauro Causa Department of Chemical Sciences, University "Federico II", Napoli, Italy

Marzio De Corato Dipartimento di Scienza dei Materiali, Universitá di Milano-Bicocca, Milan, Italy

Centro S3, CNR-Istituto Nanoscienze, Modena, Italy

Dipartimento di Fisica, Università di Modena e Reggio Emilia, Modena, Italy

Luca D'Alessio Department of Physics, Boston University, Boston, MA, USA

Maddalena D'Amore Department of Chemical Sciences, University "Federico II", Napoli, Italy

Mircea V. Diudea Faculty of Chemistry and Chemical Engineering, Babes-Bolyai University, Cluj, Romania

Massimo Fusaro Department of Chemical Sciences, University "Federico II", Napoli, Italy

Carmine Garzillo Department of Preventive Medical Sciences, University "Federico II", Napoli, Italy

Modjtaba Ghorbani Department of Mathematics, Faculty of Science, Shahid Rajaee Teacher Training University, Tehran, Islamic Republic of Iran

Ante Graovac (Deceased)

Kondayya Gundra Theoretical Physics Division, Bhabha Atomic Research Centre, Mumbai, India

Department of Physics, Indian Institute of Technology, Mumbai, India

Yezeng He Key Laboratory for Liquid-Solid Structural Evolution and Processing of Materials, Ministry of Education, Shandong University, Jinan, People's Republic of China

Ali Iranmanesh Department of Mathematics, Tarbiat Modares University, Tehran, Iran

Mohammad Ali Iranmanesh Department of Mathematics, Yazd University, Yazd, Islamic Republic of Iran

Yanyan Jiang Key Laboratory for Liquid-Solid Structural Evolution and Processing of Materials, Ministry of Education, Shandong University, Jinan, People's Republic of China

István László Department of Theoretical Physics, Institute of Physics, Budapest University of Technology and Economics, Budapest, Hungary

Jean-Pierre Leburton Beckman Institute, University of Illinois at Urbana-Champaign, Urbana, IL, USA

Hui Li Key Laboratory for Liquid-Solid Structural Evolution and Processing of Materials, Ministry of Education, Shandong University, Jinan, People's Republic of China

Yunfang Li Key Laboratory for Liquid-Solid Structural Evolution and Processing of Materials, Ministry of Education, Shandong University, Jinan, People's Republic of China

Zeinab Mehranian Department of Nanocomputing, Institute for Nanoscience and Nanotechnology, University of Kashan, Kashan, Islamic Republic of Iran

Ottorino Ori Actinium Chemical Research, Rome, Italy

Tomaž Pisanski Department of Mathematics, Faculty of Mathematics and Physics, University of Ljubljana, Ljubljana, Slovenia

Ana-Maria Putz Institute of Chemistry Timişoara of the Romanian Academy, Timişoara, Romania

Mihai V. Putz Laboratory of Computational and Structural Physical Chemistry, Biology-Chemistry Department, West University of Timişoara, Timişoara, Romania

Research Center for Einstein Physics, Institute of Theoretical Physics, Free University Berlin, Berlin, Germany

Daniel Sánchez-Portal Centro de Física de Materiales (CFM-MPC) CSIC-UPV/EHU, San Sebastián, Spain

Donostia International Physics Center (DIPC), San Sebastián, Spain

Elton J. G. Santos Centro de Física de Materiales (CFM-MPC) CSIC-UPV/EHU, San Sebastián, Spain

Donostia International Physics Center (DIPC), San Sebastián, Spain

Harvard School of Engineering and Applied Sciences, Harvard University, Cambridge, MA, USA

Cruft Laboratory, Cambridge, USA

Jelena Sedlar Faculty of Civil Engineering, Architecture and Geodesy, University of Split, Split, Croatia

Elena F. Sheka Peoples Friendship University of Russia, Moscow, Russia

Alok Shukla Department of Physics, Indian Institute of Technology, Bombay, Powai, Mumbai, India

Beata Szefler Department of Physical Chemistry, Collegium Medicum, Nicolaus Copernicus University, Bydgoszcz, Poland

Jianwei Wei College of Optoelectronic Information, Chongqing Institute of Technology, Chongqing, China

Zahra Yarahmadi Department of Mathematics, Faculty of Science, Khorramabad Branch, Islamic Azad University, Khorramabad, Islamic Republic of Iran

Hui Zeng College of Physical Science and Technology, Yangtze University, Jingzhou, Hubei, China

Jun Zhao College of Physical Science and Technology, Yangtze University, Jingzhou, Hubei, China

Chapter 1
Helical Wrapping of Graphene Sheets and Their Self-Assembly into Core-Shelled Composite Nanostructures with Metallic Particles

Hui Li, Yunfang Li, Yezeng He, and Yanyan Jiang

Abstract A series of atomistic molecular dynamics (MD) simulations have been conducted to explore how the carbon nanotube (CNT), metal nanowire (NW), and C60 affect the stability of the graphene. The graphene nanoribbons (GNRs) can helically wrap and insert the single-walled CNT spontaneously to form helical configurations, which are quite close to the helices found in nature. The graphene nanosheets (GNSs) can spontaneously self-scroll onto the Fe NWs irreversibly, which results in the structural transition of the GNS from two-dimensional to three-dimensional phase and the formation of the stable metal/carbon core-shell nanostructure. MD simulation results also show that impact of C60 molecule would induce nanoscale dynamic ripples on the graphene no matter whether the graphene is plane or corrugated. This study provides possible applications for the GNS and GNR to serve as conveyor belt for molecule delivery. And also, the discoveries of this study are of great significance for the deeper understanding of the instability and properties of graphene at an atomic level.

1.1 Introduction

Graphene nanosheet (GNS), a monatomic layer of carbon atoms arranged in a honeycomb lattice with sp^2-bonding, has attracted ever-increasing research interest since it was first isolated by mechanical exfoliation from graphite crystals (Novoselov et al. 2004). Recent experimental approaches involving mechanical cleavage (Meyer et al. 2007a), top-down lithography, cutting (Fujii and Enoki 2010) and peeling (Sen et al. 2010), chemical vapor deposition (Juang et al. 2010),

H. Li (✉) • Y. Li • Y. He • Y. Jiang
Key Laboratory for Liquid-Solid Structural Evolution and Processing of Materials, Ministry of Education, Shandong University, Jinan 250061, People's Republic of China
e-mail: lihuilmy@hotmail.com; liyf308@hotmail.com; hyz0217@hotmail.com; happylucy2006@yahoo.com.cn

and epitaxial growth (Prakash et al. 2010) have been applied to fabricate GNSs with desired sizes and shapes. Such synthesized two-dimensional (2-D) GNS may very well be the promising candidate material from electronic building blocks to reinforced composites due to its outstanding properties such as quantum electronic transport (Novoselov et al. 2005a, b), controllable electronic structure (Kim et al. 2009), large thermal conductivity (Seol et al. 2010), and extremely high elasticity (Savini et al. 2011). Recently, a number of researchers have also paid their attention to the applications of GNSs in biochemical and medical realms (Yang et al. 2008; Kalbacova et al. 2010).

The isolation of planar GNS seems to contradict the common viewpoint about the existence of 2D crystals (Mermin 1968; Ledoussal and Radzihovsky 1992). Experimental and theoretical studies have suggested that nanometer-scale ripples through the free GNS membrane might be responsible for stabilizing its 2D structure (Meyer et al. 2007b; Fasolino et al. 2007). Compared with the stable and stiff carbon nanotube (CNT), the GNS is very instable and flexible that tends to transform into a 3D structure in order to minimize its surface energy. Buehler et al. demonstrated that the geometrical conformation of the GNS is determined by its aspect ratio. When the aspect ratio is large enough, the narrow graphene nanoribbon (GNR) would self-fold from planar 2D phase to multifold or even scroll 3D phase spontaneously (Xu and Buehler 2010). Other research work also revealed the intrinsic instability and spontaneous twist of pristine GNRs (Bets and Yakobson 2009). Recent theoretical study clearly showed that the water nanodroplet had great effect on the conformation of the GNS (Patra et al. 2009), which arouses one to imagine whether other material would affect the stability of the GNS as well.

In this chapter, systematic theoretical investigations have been carried out to present the detailed analysis and explanation of how the carbon nanotube (CNT) (Jiang et al. 2011; Li et al. 2011b), metal nanowire (NW) (Li et al. 2011c, 2012), and C60 (He et al. 2011) affect the stability of the graphene.

1.2 Helical Wrapping and Insertion of Graphene Nanoribbon to Single-Walled Carbon Nanotube

In the carbon family, nanotube and graphene with a perfect honeycomb lattice tightly bounded by sp^2 hybridization are two of the most promising nanomaterials, which have attracted tremendous attention to the theoretical research and the potential applications in many realms because of their ideal 1D and 2D structures and unique properties. The cylindrical single-walled carbon nanotube (SWNT) possesses a large specific surface area and hollow interior that provide an excellent opportunity to integrate with other materials to fabricate composite nanostructures. The integration of SWNTs into other materials can impact their toughness (Zhang et al. 2003a), mechanical strength, crystalline morphology (Li et al. 2009a), and other properties like electrical conductivity. The noncovalent "wrapping" of

polymer chains around an SWNT is an interesting phenomenon (Numata et al. 2005; Naito et al. 2008) which can be utilized to solubilize and disperse SWNTs (Tasis et al. 2006; Zorbas et al. 2004), drive assembled mechanisms (Baskaran et al. 2005; Nish et al. 2007), and alter the fictionalization of the tubes (Chen et al. 2001). Moreover, previous experimental and theoretical results have shown that open nanotubes could act as "molecular straws" capable of absorbing dipolar molecules by capillary action (Pederson and Broughton 1992). On the one hand, the insertion of "foreign" materials, such as metals, liquids, fullerenes (Warner and Wilson 2010), or even proteins (Sorin and Pande 2006) and DNAs (Gao et al. 2003), into SWNTs can alter the properties of the tube and fillers, leading to nanostructures with exciting new applications. On the other hand, the carbon shell is considered as a natural protective layer of the fillers against oxidation and shape fragmentation (Choi et al. 2003). Therefore, the "SWNT composite" has great potential in heterogeneous catalysis, nanodevices, electromagnetic wave absorption, magnetic data storage, and even drug and gene delivery in biological field (Svensson et al. 2004; Gao et al. 2004).

In this section, convincing systematic theoretical results are presented to reveal how the GNR interacts with the SWNT and what is the shape of the GNR adhering onto the sidewall of the SWNT. In particular, the possible interacting mechanism is examined to establish the nature of the interaction of 1D GNR and SWNT. This study is not only helpful for the better understanding of the thermal instability and properties of GNRs at an atomistic level but also essential to help guide exploring new theories and fabricating functional nanoscale devices.

1.2.1 Simulation Method

In the present study, all calculations are carried out using molecular dynamics (MD) simulation, which is an effective tool for studying material behavior on the nanometer scale and provides detailed information at the atomic level. The force field of condensed-phase optimized molecular potentials for atomistic simulation studies (COMPASS) (Sun 1998) is applied to model the atomic interaction. The COMPASS is an ab initio force field that is parametrized and validated using condensed-phase properties in addition to various ab initio and empirical data. It aims to achieve high accuracy in prediction of the properties of very complex mixtures (Bunte and Sun 2000; Li et al. 2011a), and it has been proven to be applicable in describing the mechanical properties of graphene sheets (Zheng et al. 2010). MD simulations are performed under an NVT ensemble (i.e., the canonical ensemble, the number of particles N, the volume V, and the temperature T were constant) at temperature 300 K. The Andersen method in the thermostat is applied to control the temperature and generate the correct statistical ensemble. The thermodynamic temperature is kept constant by allowing the simulated system to exchange energy with a "heating bath." The initial velocities of carbon atoms follow a temperature-dependent Maxwell-Boltzmann distribution, and the Verlet algorithm

is adopted to integrate the motion of equations of the whole system. The time step is set to be 1.0 fs, and data were collected every 5.0 ps to record the full-precision trajectory for further analysis. Each of the GNR-SWNT systems was simulated long enough to achieve an equilibrium state. The SWNTs were fixed as rigid tube structures. The GNRs can be cut from the parallel layers in graphite bulk, and so some of GNRs have open edges with dangling σ-orbitals on carbon atoms, whereas the others are not due to the π–π stacking interaction between adjacent layers. Initially, all GNR crystals were placed at the entrances of the SWNTs along the axial direction and overlapped 15 Å with the SWNTs to overcome the deformation force from the GNRs themselves and ensure that the distances between them are in the range of the cutoff distance of vdW interaction. To illustrate the interaction process more clearly, the long sinuous GNR tails were not shown.

1.2.2   Results and Discussion

1.2.2.1   Helical Wrapping and Insertion

Direct simulations in Figs. 1.1 and 1.2 provide the representative snapshots of a GNR helically wrapping onto the SWNT (16, 16) and inserting into the SWNT (20, 20), respectively. Two SWNTs have the same lengths of 66.41 Å. The size of GNR is 500.61 Å in length and 7.81 Å in width. When one end of the GNR is captured by the SWNT (outer or inner surface) and the deformation force from the GNR itself is overcome, the GNR adheres onto the tube wall parallel owing to the vdW coupling and moves toward the tube. When the simulation begins, the GNR is so thin that it tends to be thermodynamically unstable, becoming discontinuous wrinkles or corrugations at thicknesses of several nanometers, which accords well with Yakobson et al.'s result (Bets and Yakobson 2009). It is believed that the planar GNR is easily twisted or bent in a free space because of edge stress. As a result, the GNR assumes polymer-like chain conformation. Although the corrugations and ripples are intrinsic to graphene membranes and stabilize their 2D structures (Fasolino et al. 2007), the 1D wavy fluctuation in narrow GNR is rather than the 2D ripples in graphene membrane. It is mainly because when an out-of-plane bending deformation along one direction is formed, the resistance to bending along another direction will be significantly enhanced.

As the simulations progress, the GNRs start to move forward along the sidewalls of SWNTs gradually in a straight or helical mode after an initial correlation time, in which the GNRs are held tightly against the sidewalls of SWNTs and the wrinkles vanish because of the interaction between them. When the simulation time is up to $t = 8$ and 4.5 ns, the GNRs display clear helical conformations on the surface and in the hollow interior of the SWNTs with large pitch, respectively, trying to occupy the entire tubes. Then, spirals become denser because of the vdW binding. The GNR heads are pushed to move forward circumferentially owing to the curvature of the tube wall, and the ribbon tails just continue to wrap or encapsulate the tubes in

Fig. 1.1 Representative snapshots of a GNR helically wrapping onto the SWNT (16, 16). The long sinuous GNR tails are removed for better visualization. The *inset* is the top view of the snapshot at $t = 28$ ns
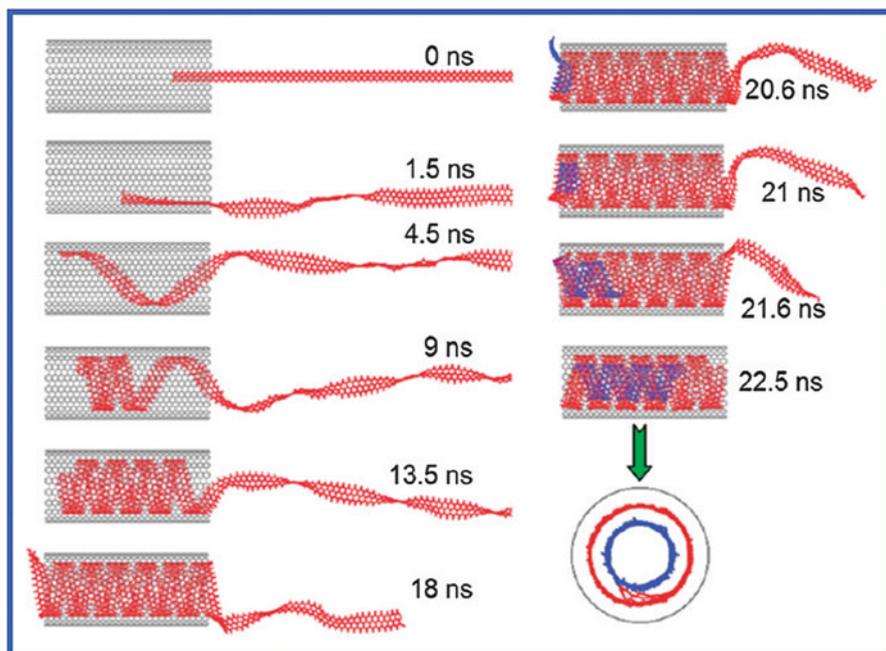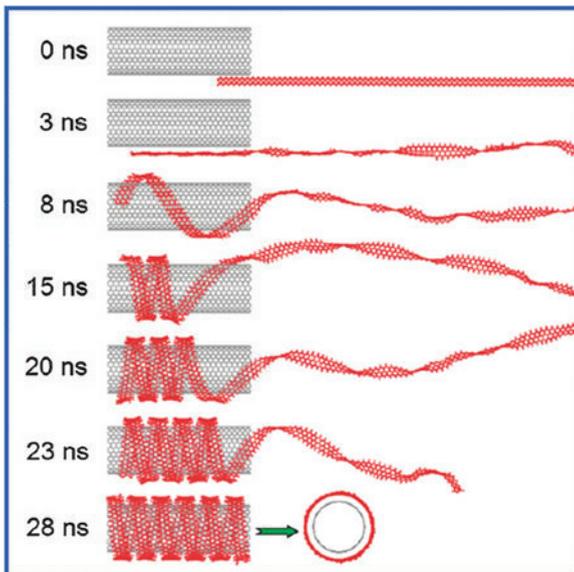

Fig. 1.2 Representative snapshots of a GNR helically inserting into the SWNT (20, 20). The new helix in the former one is marked *blue*. The long sinuous GNR tails are removed for better visualization. The *inset* is the top view of the snapshot at $t = 22.5$ ns

a helical way. Eventually, perfect circular GNR helices, with remarkably constant pitches and constant value 3.5 Å of the gap between neighboring spiral, wrap around and fill up the SWNTs at $t = 28$ and 18 ns, respectively. The self-assembled GNR-SWNT systems achieve their dynamic equilibrium through spontaneous wrapping and encapsulation. These two helix-forming processes are irreversible no matter whether the final GNR-SWNT composite nanostructures are cooled or heated to any point of temperature. The handedness of the GNR helix is determined by the initial deflection of the captured end, which can be right- or left-handed with equal probability. It can be controlled by a small initial angle between the GNR and the tube axis.

These helical GNR structures are quite close to the helices found in nature. The GNR helix wrapping around the SWNT is quite similar to the soft stem of the scammony (such as morning glory) helically climbing around the trunk to make itself strong and grow upward, whereas the GNR helix encapsulating in the SWNT is just like a spirogyra cell in which the chloroplast ribbon grows helically over its whole length to make the photosynthesis and the starch storage more efficient (Ohiwa 1976). Perhaps these coincidences with the natural phenomenon can bring some enlightenment on a broad new class of potential applications of these helical carbon nanostructures. Moreover, helicity is one of the essential features of life and integral to various biological functions. In biological systems, various important substances such as polypeptides and DNA in confining cells are found to present helical structures. It is believed that helicity is intimately associated with the living processes even though their origin remains unclear.

It is worth noting the subsequent evolution of the inserting process in Fig. 1.2 when the interior of the SWNT is fully filled. As the simulation goes on, the GNR tail is not stopping but continues to enter the SWNT helically. The head of the helix in the SWNT is pushed out a bit by the tail, but it is not possibly completed because the vdW attractive force from the tube is strong enough to trap the GNR helix. It is very interesting that the pushed out GNR head is captured by the inner hollow space of the GNR helix (marked blue at snapshot of $t = 21$ ns) instead of forming new segment of the helix due to the attractive force from the inner space of GNR helix, whereas the ribbon tail just keeps on encapsulating into the SWNT helically. The captured GNR head inserted into the hollow space of the former helix also follows the helical manner and finally produces a new helix with opposite handedness (marked blue), becoming a double-shelled helix at the other entrance of the SWNT at $t = 22.5$ ns. (The inset is the top view.) The result suggests that the attraction between the GNR helix and the SWNT is stronger than that between GNR helices.

1.2.2.2 Interaction Mechanism

What we are concerned with is why the GNR moves toward the SWNT and develops a helical manner. Generally speaking, for a single GNR, as in the polymer chains, there is a persistence length $l_P = DW/k_B T$ for the width W, where D is the bending rigidity of the GNR, k_B is the Boltzmann constant, and T is the temperature.

Therefore, the critical aspect ratio for a GNR is $n = l_P/W = D/k_BT$. When the aspect ratio is smaller than n, the GNR will exhibit a worm-like chain conformation, whereas if the aspect ratio is beyond this value of n, then the GNR will tend to fold into 3D labyrinthic wedge, loop, or scroll nanostructures spontaneously, driven by thermal fluctuation and the loss of orientational order. From our theoretical estimate, the critical aspect ratio is not accessible $n = 34$ for GNR with width 7.81 Å at room temperature and that of the GNR we chose ($n = 64$) is greatly in excess of this value. However, when the GNR is introduced to SWNT, the GNR helix is formed on the inner or outer surface of the SWNT.

There should be three main interaction effects that exist between the GNR and the SWNT during the helical wrapping and insertion processes. The first effect results from the vdW interaction between the GNR and the SWNT that drives the GNR continuously moving toward the tube, and the well-known vdW potential well of the SWNT traps the GNR. To reveal the energy evolution and the role of the vdW interaction quantitatively, we give in Fig. 1.3 the evolution of the potential energies (E_P) of the above-mentioned two GNR-SWNT systems and the vdW interaction energies (E_{vdW}) between GNRs and SWNTs against time. During the whole helix-forming courses, the potential energy of these two GNR-SWNT systems appears to be in steady decline with the simulation times, indicating that the helical wrapping and insertion of GNR to SWNT are spontaneous and the systems gradually reach more stable states. Increase in the contact area between the GNR and SWNT reduces the systematic potential energy and enhances the stability of the GNR-SWNT system. Then, the two systems reach the lowest energy states; thereafter, the systemic potential energies remain unchanged, suggesting that the whole systems are in their equilibrium states. It is worth mentioning that in the potential energy curve of inserting process (Fig. 1.3b), there is a "platform" after the tube is fully filled owing to the fact that the contact area between GNR and SWNT is virtually unchanged; then, a "rapid drop" after the ribbon head is captured by the inner space of the former GNR helix because of the increase in the contact area between two GNR helices, which also enhances the stability of the GNR-SWNT system.

From Fig. 1.3, the vdW interactions are negative, suggesting that the vdW interactions between the GNRs and SWNTs are attractive. The vdW attraction energy increases nearly linearly with the increase in the contact areas until the GNRs fully wrap onto or insert into the SWNTs, which endows the GNRs with kinetic energy and sustain the continuous wrapping and insertion. Moreover, the variations of vdW attraction energies are nearly synchronous with that of potential energies, respectively. Therefore, we suggest that the vdW interaction between the GNR and the SWNT offers the main driving force to drive the GNR continuously moving toward the SWNT. The vdW attraction energy reaches up to -1.70 and -2.25 Mcal/mol, respectively, indicating that the adhesion is so strong that it is hard to strip the GNRs off the SWNTs to recover their planar structures again.

The second effect should be the offset face-to-face $\pi-\pi$ stacking interaction between GNR and SWNT (Głóbwka et al. 1999; Hunter and Sanders 2009), which is an intermolecular interaction in the paralleled six-membered rings, which causes the GNRs to be held tightly against the sidewalls of the tubes and take a helical shape. In the GNR-SWNT system, the offset face-to-face $\pi-\pi$ stacking interaction
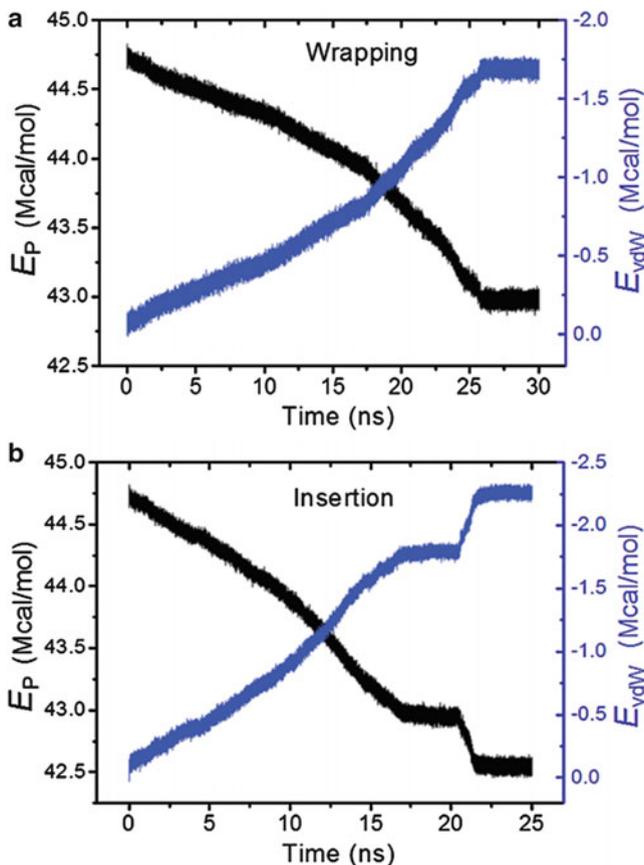
Fig. 1.3 Potential energy (E_P) of GNR-SWNT system and the vdW interaction energy (E_{vdW}) between the GNR and SWNT as a function of simulation time: (**a**) helical wrapping and (**b**) helical insertion

contains two kinds of interactions: the π–π electron interaction and the π–σ interaction. The π–π electron interaction is an important repulsive force, which is roughly proportional to the area of π-overlap of the two six-membered rings. Certainly, displacement of the interaction system diminishes the repulsion. The π–σ interaction is an attractive force between π electrons of one ring and the σ-framework around the inner edge of the cavity of the other one. Different from π–π electron interaction, this attractive interaction can be maximized in displaced stacking. Furthermore, in a stacking system, stacked structures should be exactly parallel to reduce the repulsion and increase the attraction of the π-system. It must be pointed out that the π–π stacking interaction along the radial direction, of course, does not affect the GNR to move freely along the axial and circumferential directions of SWNT. Therefore, the best way to keep the displaced stacking,
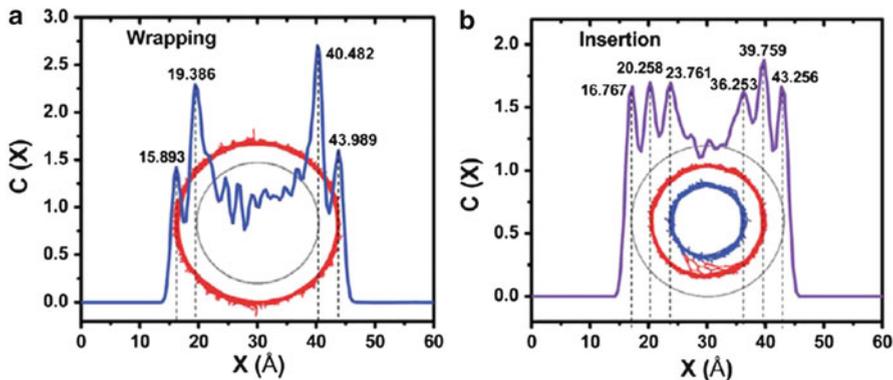
Fig. 1.4 Concentration distribution profiles of the final GNR-SWNT configurations in the *X* direction. Inserts are peak values: (**a**) helical wrapping and (**b**) helical insertion

perfect parallel, and the most contact area in the GNR-SWNT system is that the arrangement of the GNR follows a helical mode adhering onto the sidewall of the SWNT when increasingly longer GNR is trapped on the surface and inside the tube. Moreover, the displacement of the carbon rings favors to minimize the repulsive $\pi-\pi$ interaction and maximize the attractive $\pi-\sigma$ interaction with the sidewall of tube in GNR helix with paralleled arrangements of six members with SWNT. To testify the effect of the $\pi-\pi$ stacking interaction further, we characterize the geometric parameters of the final GNR-SWNT configurations by the concentration distribution profiles in the *X* direction, as shown in Fig. 1.4. From the peak details marked in the insets, the distances between the helices and the SWNTs as well as those between two GNR helices inside the tube are close to 3.5 Å, which accords well with the parallel stacking distance of the offset face-to-face $\pi-\pi$ stacking interaction (Głóbwka et al. 1999; Hunter and Sanders 2009), proving that the $\pi-\pi$ stacking interaction plays a dominant role in the helical wrapping and insertion processes.

The third most important effect is the dangling σ-orbitals on carbon atoms at the open edges of GNR, which reinforces the $\pi-\pi$ stacking interaction in GNR-SWNT system through the extra attraction with the π electrons in the sidewall of the SWNT (Głóbwka et al. 1999) that ensure that the arrangement of the GNRs follows a helical mode. In a planar sp^2 graphene system, the electronic states split into in-plane (σ) and out-of-plane (π) states that are decoupled by symmetry. At unsaturated zigzag edges, the hexagonal carbon network is interrupted, and both the σ and the π systems form edge states. The edge states of the σ system are unpaired electrons in sp^2 orbital, which are dangling σ bonds. To reveal the effect of the dangling σ-orbitals, we also studied the interactions between the SWNTs and GNRs with no dangling σ-orbitals (NGNRs). After the NGNR head attaches onto the tube (inner or outer wall), although the vdW attraction and the $\pi-\pi$ stacking interaction still work, the NGNR tends to ignore the existence of the SWNT and

form labyrinthic stacks, just like the self-folding of a free GNR (Xu and Buehler 2010). The interaction process is uncontrollable, and the final structure is very random. We also simulate the interactions between SWNT and NGNR when the dangling σ-orbitals on carbon atoms are substituted or saturated by hydrogen atoms, but there is still no helix forming. We think it is mainly due to the fact that the drive force is the vdW interaction between the NGNR layers rather than that between the SWNT and NGNR because the π−π stacking interaction between the SWNT and the NGNR is so weak that it cannot overcome that from the NGNR itself.

However, under the guidance of the GNR with dangling σ-orbitals on carbon atoms at the open edges, the NGNR can also form a helix, as shown in Fig. 1.5. The lengths of the zigzag SWNTs (28, 0) and (35, 0) are 73.13 Å, and two GNRs are both with 260.76 Å in length. In the wrapping process (Fig. 1.5a), two GNRs are placed at one entrance of SWNT and 6 Å away from the tube wall. Two GNRs move forward; then, the GNR with open edges starts to fold helically at $t = 3.5$ ns first and guides the other one to wind. The possible cause should be that open edges reinforce the π−π stacking interaction with the SWNT through the extra attraction between dangling σ-orbitals on carbon atoms of the open edges and the π electrons in the sidewall of the SWNT. Up to $t = 7$ ns, helices arise to both the ribbons, and the two tail layers contact each other because of the π−π interaction. As the MD simulation goes on, the GNR with open edges is gradually separated from the other one because of the extra attraction with tube wall. Finally, two GNRs form a double-helix structure on the tube surface, which closely resembles the double-stranded DNA. In the inserting process (Fig. 1.5b), two GNRs are separated from each other 15 Å away at one entrance of SWNT. As the simulation begins, the GNRs adhere onto the tube wall rapidly, whereas the parts outside the tube contact each other because of the π−π interaction between two layers. We suggest that the π−π stacking interaction in the GNR-SWNT system should be stronger than that between two GNR layers. As time goes on, the GNR with open edges is gradually separated from the other one mainly because of the extra attraction between dangling σ-orbitals on carbon atoms of the open edges and the π electrons in the sidewall and forms the helical configuration earlier. Consequently, a DNA-like double helix is also constructed inside the SWNT at $t = 7.5$ ns. When time progresses, two GNR tails also enter the inner space of the double helix to produce new helices, becoming a double-shelled helix in the tube, which accords well with the encapsulation of one GNR into the tube (as shown in Fig. 1.2). From our calculations, two equilibrated GNRs in double helix always have the same handedness. The results indicate that the driving force of the formation of double helix should be the vdW interaction between the SWNT and GNRs. Therefore, the dangling σ-orbitals on carbon atoms at the open edges play an important role in the helix forming of the GNRs during the interaction with SWNTs.

The cylindrical structure of the SWNT is also very important in the helix-forming process, which provides uniform curvature to make the GNR move along the circumferential direction of SWNT. Furthermore, the high flexibility dependent on the perfect hexagonal honeycomb architectures and the intrinsic instability (Xu and Buehler 2010; Bets and Yakobson 2009) of the GNR has also contributed to the formation of the GNR helix. The rigid MoS_2 inorganic nanoribbon encapsulated
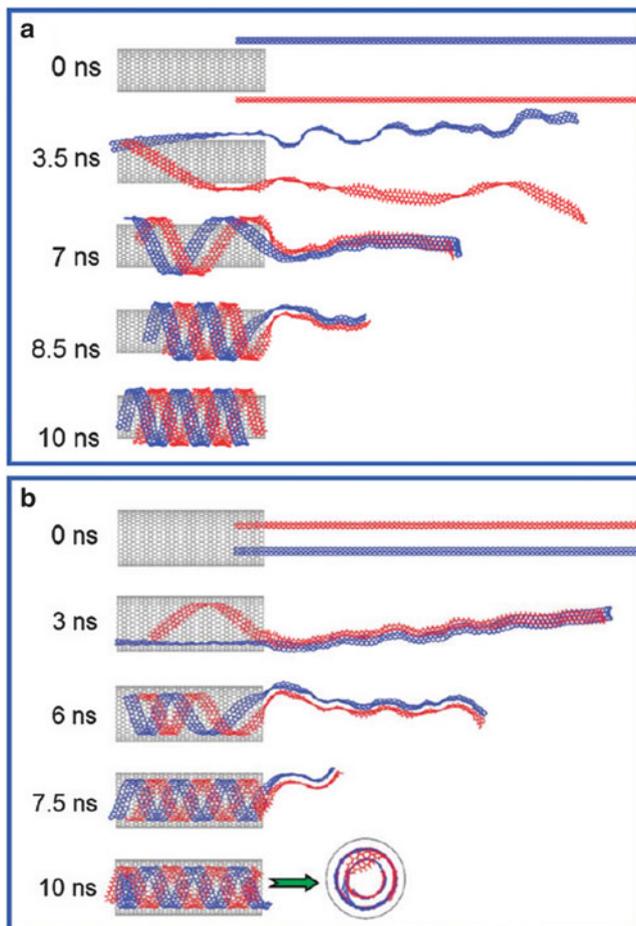
Fig. 1.5 Evolution snapshots of two GNRs interacting with SWNT. (**a**) Helical wrapping of GNRs onto the SWNT (28, 0) and (**b**) helical insertion of GNRs into the SWNT (35, 0). The *inset* in part **b** is the top view of configuration at $t = 10$ ns

in single- and double-walled carbon nanotube can only display planar conformation (Wang et al. 2010). Experimental results of Snir and Kamien (2005) are very helpful for better understanding this unique phenomenon. Snir and Kamien constructed the system as a flexible, unbreakable solid tube immersed in a solution of the mixture of hard spheres, and they found that the best shape of the short flexible tube that takes the least amount of energy and takes up the least space is a helix with a geometry that is close to that of the helices found in nature. Other theoretical result also revealed that the heterogeneous nucleation of silicon occurred on carbon nanocones preferred to follow a spiral mechanism (Li et al. 2009b). Therefore, we suggest that the helical wrapping and encapsulation of GNR to the SWNT perhaps are because the GNR helix takes the least amount of energy and is a natural space saver.
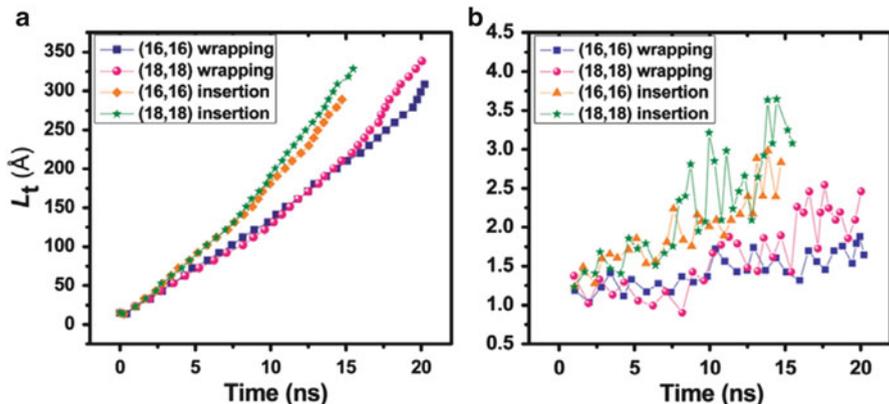
Fig. 1.6 Variations of the ribbon length adhered onto the SWNTs L_t and the instantaneous velocities V_t against time during the GNR wrapping and inserting the SWNTs (16,16) and (18,18), respectively. (**a**) Ribbon length versus time and (**b**) instantaneous velocity versus time

1.2.2.3   Dependence of Size, Chirality, and Integrality

To exploit the effect of SWNT diameters on the interaction character between GNR and SWNT deeper, we give in Fig. 1.6 the variations of the ribbon length L_t adhered onto the SWNT and the instantaneous velocity V_t relative to the tube entrance versus time t during the GNR helically wrapping and inserting SWNTs (16, 16) and (18, 18) with lengths 73.79 Å. The GNRs are all placed 6.0 Å away from the sidewalls of SWNTs and overlapped 15.0 Å with the SWNTs. The speed is determined by the strength of vdW forces acting on the GNR and the rate of its momentum dissipation due to friction with the sidewall of SWNT. As shown in Fig. 1.6a, the changes of L_t display nonlinear dependence on time t, indicating that the helical wrapping and insertion are not uniform motions. It should be pointed out that because of the deformation force, the GNR pulls out a bit from the SWNT but bounces back very soon owing to the attraction from the tube. Then, the velocity of GNR reaches its intrinsic speed. From Fig. 1.6b, it is seen that the velocities of the GNRs inserting into the SWNTs are obviously higher than that of those wrapping onto the SWNTs owing to stronger vdW attraction from the interior confining space of the tube, which accelerates GNRs to encapsulate into tubes. However, the velocity of the GNR in wrapping or inserting the SWNT with larger diameter is only slightly higher than that in the SWNT with smaller diameter. It is worth noting that all velocities show an increase in their tendency with time except for some fluctuations. In fact, the motion of GNRs is a variable accelerated motion because the attractive force from the tubes remains virtually unchanged, while the mass of the unattached GNR tails keeps decreasing, which can also be reflected from the change rate of the E_P and E_{vdW}.

To realize the control to GNR helix, a key issue crucial to know is that of the dependence of the diameter and chirality of SWNT as well as the width of GNR in the helix-forming process. In the helical wrapping, the GNR can wind onto any kind of SWNTs spontaneously and form GNR helix, even the ultrathin SWNT (4, 4) with the diameter only 5.42 Å. As shown in Fig. 1.7a, the helical wrapping of the GNR is slightly dependent on the diameter and the chirality of SWNT. Figure 1.7b illustrates the effect of the width of GNR on the helical wrapping. The width of the narrowest GNR with open edges is 5.681 Å in which it contains only one string of carbon six-membered rings. The GNRs with different widths can helically wrap onto the SWNT (15, 15) because the exterior of the SWNT is free and the motion of GNR is not confined.

However, the situation of the helical insertion is much more complex because of the confinement of tube wall. The encapsulation of GNR into SWNTs with different diameters and chiralities is simulated to deeper clarify, just as shown in Fig. 1.7c. If the SWNT with diameter is not larger than 10.85 Å (for instance, the armchair SWNT (8, 8)), then the GNR cannot encapsulate into the tube, even the narrowest GNR with width of 5.681 Å. With a slight increase in the diameter of the SWNT, although it can fill the tube, the narrowest GNR just keeps planar or twisted because the inside space is so confined that the helix cannot form, as seen by the GNR in the armchair SWNT (9, 9). From our calculations, if the diameter of the SWNT is in the range from 13.31 to 14.92 Å, then the narrowest GNR with 5.681 Å in width can form a helix with a large pitch in the tube to take up as much as space and keep the whole system stable, as shown by the GNR in the zigzag SWNT (17, 0). Only when the diameter reaches 14.92 Å (the armchair SWNT (11, 11)) can the GNR produce a perfect helix inside the nanotube. Just as seen in Fig. 1.7c, the perfect GNR helix can be formed in the SWNTs with different chiralities when the diameter of SWNT is $\geq$14.92 Å. Our calculations indicate that the helical encapsulation of the GNR into the SWNT is strongly dependent on the tube diameter but slightly dependent on the tube chirality. To investigate the effect of the GNR width, as shown in Fig. 1.7d, we found that the width of GNR W that ensures the helical insertion of the GNR into a given SWNT should be narrower than the threshold value $W_{into} = D - 2 \times 3.5$ Å, where D is the diameter of the tube and 3.5 Å is the optimized distance of the interaction between carbon atoms. If the GNR is a bit wider than the maximum W_{into} and a little narrower than D, then the helical structure will still be formed during the encapsulation process when the GNR can self-adjust well through slight bend or twist, but it is much more difficult and uncertain. Therefore, for a given SWNT with the diameter larger than 14.92 Å, to ensure a perfect GNR helical structure to be formed in the encapsulation process, it should satisfy the fact that the width of the GNR is in the range of 5.681 Å and the threshold value W_{into}. In all GNR helices, the gap between neighboring spirals is a constant value of 3.5 Å, so the pitch of the GNR helix P is only determined by the width of the GNR that $P = W + 3.5$ Å. Therefore, we can control the GNR helix by the SWNT diameter and the GNR width.

To clarify quantitatively the influence of the chirality and diameter of SWNT on the adhesion of GNR-SWNT system, we have further determined the saturation interaction energies per unit area ΔE between a GNR and the SWNTs with different
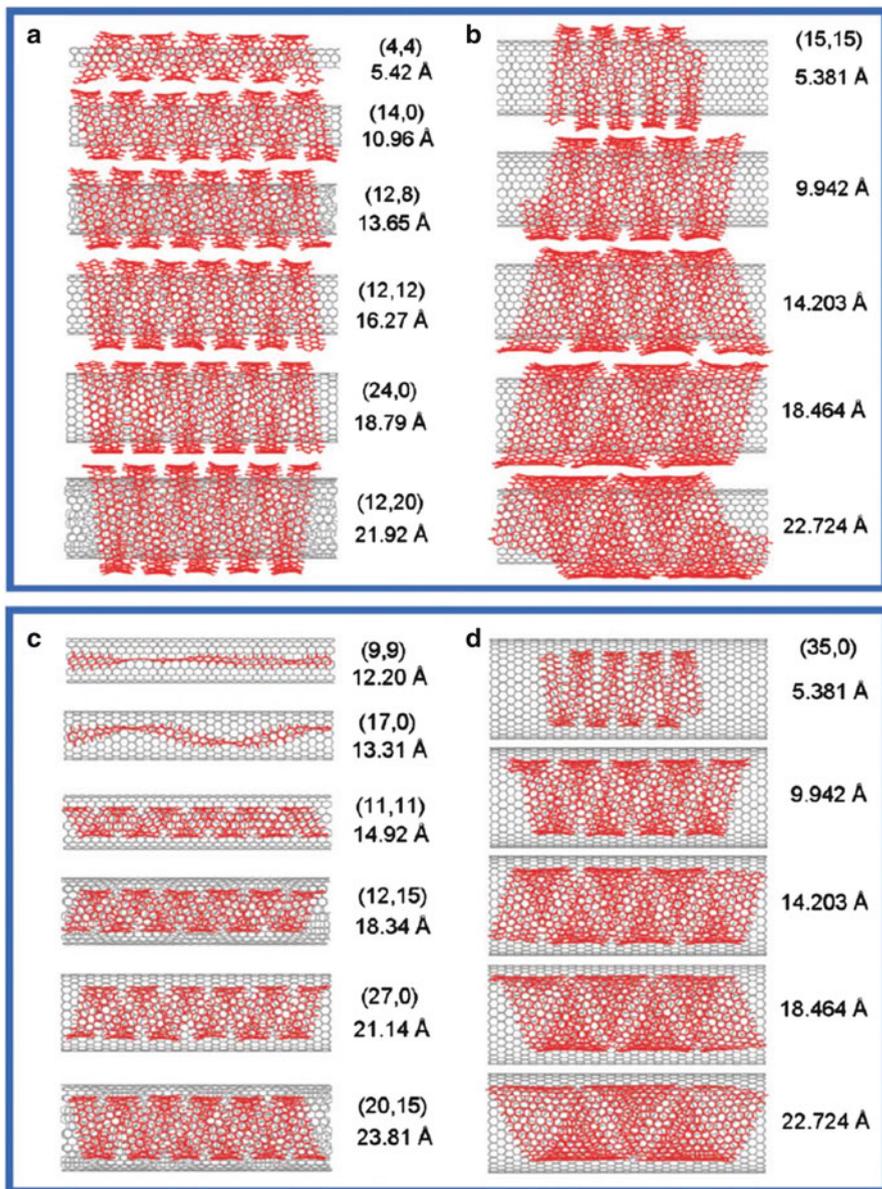
Fig. 1.7 Dependence of the diameter and chirality of SWNT and the width of GNR in the helix-forming process. (**a**) Helical wrapping of GNR onto the SWNT with different diameters and chiralities, (**b**) helical wrapping of GNR with different widths onto the SWNT (15, 15), (**c**) helical encapsulation of GNR into the SWNT with different diameters and chiralities, and (**d**) helical encapsulation of GNR with different widths into the SWNT (35, 0)
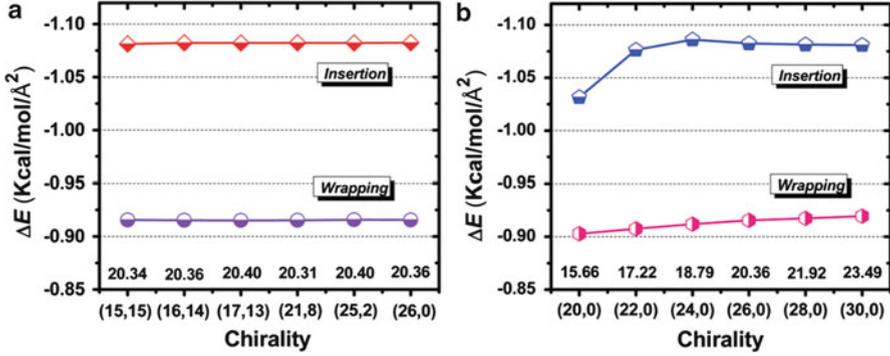
Fig. 1.8 (**a**) Saturation interaction energies per unit area between the GNRs and the SWNTs with different chiralities. (**b**) Saturation interaction energies per unit area between the GNRs and zigzag SWNTs with different diameters

chiralities and diameters showing in Fig. 1.8. ΔE reflects the adhesion intensity between the GNR and SWNT that can be calculated from the following equation:

$$\Delta E = \frac{E_{\text{total}} - (E_{\text{GNR}} + E_{\text{SWNT}})}{A_{\text{GNR-SWNT}}} \tag{1.1}$$

where E_{total} is the total potential energy of the optimized GNR-SWNT system, E_{GNR} is the intrinsic energy of the single GNR without SWNT, E_{SWNT} is the minimum energy of the isolated SWNT without GNR, and $A_{\text{GNR-SWNT}}$ is the contact area between the GNR and SWNT. From Fig. 1.8a, we can observe that the ΔE between the GNR and SWNTs with different chiralities remains almost constant, indicating that the SWNT chirality has a negligible influence on the adhesion. It further verifies the fact that the helical wrapping and insertion depend slightly on the tube chirality. The insets are the diameters of SWNTs. However, when the GNR helix is in the hollow interior, the ΔE is obviously higher than that of the GNR helix on the exterior of the SWNTs, suggesting that the GNR helix in the hollow interior is more stable than that on the outer surface of the SWNT. It is mainly because the vdW potential well inside the SWNT is deeper, therefore, providing more vdW attraction than that from the exterior of the tube. Figure 1.8b shows that the diameter of SWNT has a great effect on the adhesion. When the GNR wraps onto the SWNT, the ΔE is increased with the increase in the tube diameter linearly, proving the fact that the more flat the SWNT wall (lower curvature), the stronger the adhesion intensity between GNR and SWNT. However, in the case of insertion, the ΔE increases firstly and then reaches to an equilibrium value with no effect of the tube curvature.

We have further simulated the dependence of the integrality of SWNT on the helical wrapping and insertion. We make the gap on SWNT by deleting the carbon atom chains along the axial direction to destroy the continuity of the tube wall. The edges of gaps are marked blue. The GNRs are all 300.12 Å in length and placed
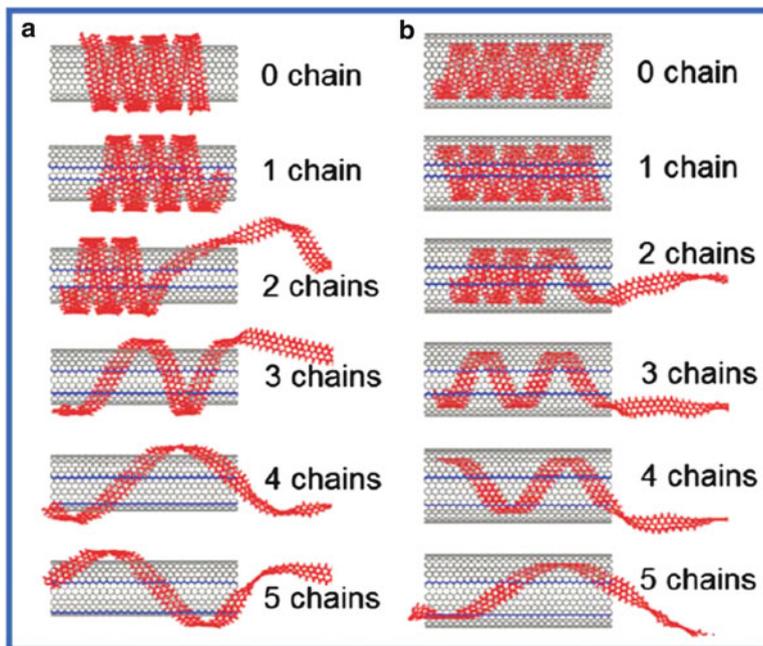
Fig. 1.9 Effect of the gap of SWNT on the helix-forming process. The edges of gaps are marked *blue*. (**a**) Helical wrapping of GNR onto the SWNTs (15, 15) with gaps. (**b**) Helical encapsulation of GNR into the SWNT (20, 20) with gaps. *Insets* are the number of carbon atom chains that the gap contains

in the same location in all initial configurations. Figure 1.9 shows configurations of the GNR wrapping onto the SWNTs (15, 15) and inserting into the SWNTs (20, 20) with gaps at $t = 13.5$ and 10 ns, respectively. The insets are the number of carbon atom chains that the gap contains. Figure 1.9 demonstrates that the small gaps (containing 1 chain) have no obvious effect, whereas the larger gaps on the tube walls slow or impede the helical wrapping and insertion. It could be seen that the gap that contains four chains stops the helical wrapping, whereas the gap that contains five chains stops the helical insertion. It is mainly because the motion of GNR along the circumferential direction depending on the curvature of the tube wall is destroyed. So the integrality of SWNT is also very important for the helical wrapping and insertion of the GNR.

1.2.2.4 Possible Application

The unique phenomenon that the GNR can helically wraps onto and encapsulates into the SWNT spontaneously inspires our interests to utilize the GNR as nanoscale vehicle to deliver molecules onto the surface or into the confining nanospace of tube,

respectively. On one respect, the surface of SWNTs is often chemically modified to reach proper dispersion and compatibility (Khan et al. 2007). However, chemical modifications will create defects in the external wall of the SWNTs and affect their properties (Sulong et al. 2009). The spontaneous wrapping of GNR may be the more gentle approach to modify the SWNT, and attached molecules on the outer surface may guide the tube to a specific target. On the other respect, the larger inner confined volume of the SWNT can be used as the drug container and targeted delivery capsule (Hilder and Hill 2009). The spontaneous insertion of the GNR can carry the molecules into the confining nanospaces of tubes without any other external force. In this simulation, we chemically attach some norepinephrine molecules to the GNRs with length of 300.12 Å uniformly. The norepinephrine is an important drug in biology and medicine that has a key neurotransmitter function in the human organism to regulate motor coordination, behavior, learning and memory, sleep-wake cycle, and stress response (Zhu et al. 2010; Nagy et al. 2003; Zhou et al. 2007). Just as shown in Fig. 1.10, the norepinephrine-modified GNRs gradually wrap (Fig. 1.10a) and insert (Fig. 1.10b) the SWNTs to form the helical configurations. The attached molecules have a comparatively small impact on the helix-forming process and the interval between the neighboring segments. Besides norepinephrine, other drugs, catalysts, enzymes, and functional groups can also be attached to the GNR and easily carried to the exterior or interior of SWNTs. We can easily manage the amount of the modified and encapsulated molecules and locate them at the specified positions for a given SWNT because it is easy to know the pitch of GNR helix and the distance between the tube and the helix and that of the neighboring spirals. Then, we can distribute the required molecules according to the individual requirement and make full use of the spontaneous and helical properties of the GNR when GNRs interact with SWNTs. Therefore, the GNR can be a promising nanoscale vehicle to deliver substances, and the GNR-SWNT system is expected to explore numerous prospective chemical and biological applications.

1.3 A Graphene Sheet Spontaneously Scrolling Round an Iron Nanowire

The structures and properties of NWs are quite different from those of bulk materials owing to the strong impact of the surface. Because of magnetic performance, iron (Fe) NWs are studied intensively, and various techniques have been developed for the production of long and regular Fe NWs. Highly ordered Fe NWs with diameters of several nanometers have been fabricated by the decomposition of a suitably chosen perovskite (Mohaddes-Ardabili et al. 2004), electrodeposition using porous alumina templates (Zhang et al. 2003b; Borissov et al. 2009), and iron deposition on suspended CNT substrates (Zhang and Dai 2000). Moreover, Fe NWs of atomic size can be generated using CNTs (Demoncy et al. 1998) or polymer (Thurn-Albrecht et al. 2000; Hong et al. 2001) and biological templates like DNA (Seidel et al. 2002).
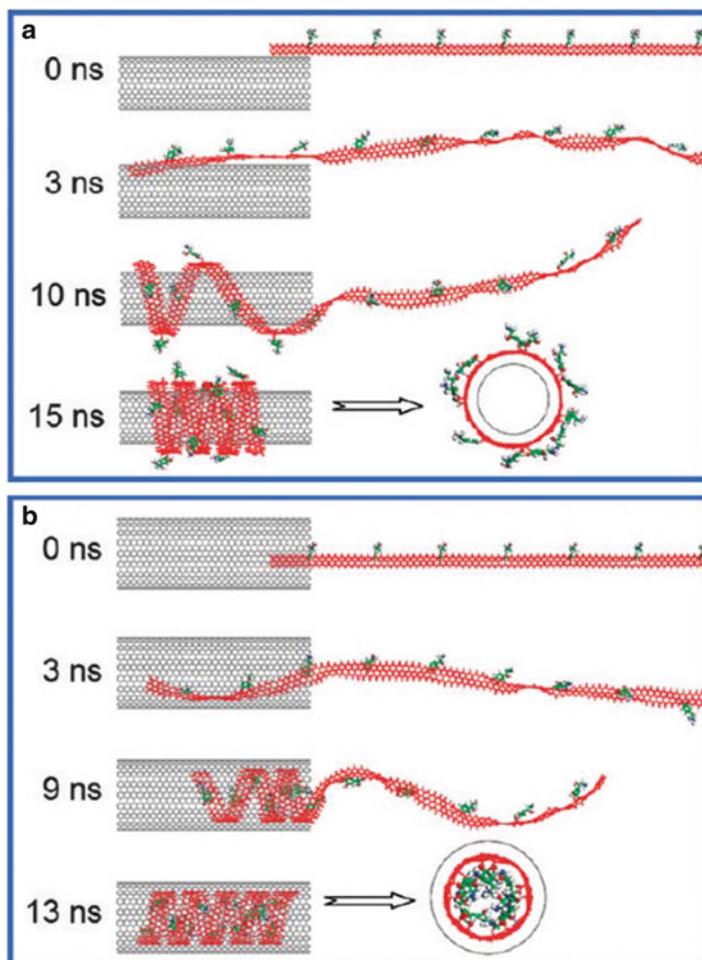
Fig. 1.10 Evolution snapshots of the GNR modified with norepinephrine molecules interacting with the SWNT. (**a**) Helical wrapping of modified GNR onto the SWNT (15, 15); (**b**) helical encapsulation of modified GNR into the SWNT (20, 20). The *insets* are the top views of final configurations

Although there have been a large number of important research studies on the stability and properties of GNS, the study of the interaction between the GNS and a metallic NW is still limited. Understanding their interacting mechanism is of great importance in exploring the practical applications of GNSs and fabricating new composite functional materials (Potts et al. 2011; Goswami et al. 2011).

In this section, theoretical results are presented to reveal that GNSs can fully self-scroll onto Fe NWs to produce magnetic core-shell nanostructures, which can be potential candidates for use in nanodevices, in wave-absorption materials, and

in the magnetic storage industry. In particular, the interacting mechanism and the thermodynamic model are examined to establish the nature of the spontaneous scrolling of GNS. This study is not only helpful for the better understanding the thermal instability and properties of GNS at an atomic level but essential to expand the practical application of GNS and explore new theories and functional devices.

1.3.1 Simulation Method

In this work, all calculations are also carried out by MD simulation, and the atomic interaction is described by the force field of COMPASS. The MD simulations are performed under an NVT ensemble at room temperature of 300 K. The Nose method is employed in the thermostat to control the temperature and generate the correct statistical ensemble. The thermodynamic temperature is kept constant by allowing the simulated system to exchange energy with a "heating bath." The Verlet algorithm is adopted to integrate the equations of motion for the whole system. The time step is set to be 1.0 fs, and data were collected every 0.1 ps to record the full-precision trajectory for further analysis. The cylindrical Fe NWs are prepared in body-centered cubic crystal structure of Fe (Sandoval and Urbassek 2009; Yan et al. 2009; Opitz et al. 2002) and the wire axes oriented in the (001) direction with radius range from 5 to 10 Å in order to maintain their small size effect and structural stability. It has also shown that a wire radius favors for larger than a critical radius with cross section of about two to seven atoms, in dependence on the used metallic element (Kondo and Takayanagi 1997; Wang et al. 2001; Gulseren et al. 1998). Below this critical radius, the wire structure is helical (Kondo and Takayanagi 1997; Wang et al. 2001; Gulseren et al. 1998; Kondo and Takayanagi 2000). Initially, the width of a GNS aligns parallel to the Fe NW and with a separation distance of 8.0 Å. Each system is simulated long enough to achieve an equilibrium state.

Because Fe is a transition metal, the spin-unrestricted density function theory (DFT) is performed to study the interaction between Fe and carbon on the GNS. The DFT computations are carried out through an all-electron method with a generalized gradient approximation (GGA) for the exchange-correlation term. The double numerical basis set including the d-polarization functions (DND) basis set and PW91 (Perdew and Wang 1992) functional is adopted. A convergence criterion of 10^{-6} au on the total energy and electron density is adopted for the self-consistent field (SCF) calculations. The real-space global orbital cutoff radius is chosen as 4.6 Å. The Brillouin zone is sampled with $3 \times 3 \times 1$ k-points. The transition state is located through the synchronous method with conjugated gradient refinements (Govind et al. 2003). This method involves linear synchronous transit (LST) maximization, followed by repeated conjugated gradient (CG) minimizations, and then quadratic synchronous transit (QST) maximizations and repeated CG minimizations until a transition state was located.

Fig. 1.11 Snapshots of the spontaneous self-scrolling of a GNS onto a Fe NW
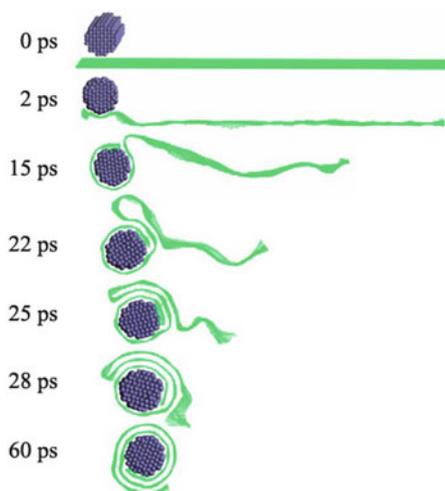
1.3.2 Results and Discussion

1.3.2.1 The Spontaneous Scrolling of GNS

Direct simulation in Fig. 1.11 provides snapshots of the spontaneous scrolling of an armchair GNS with size of 207.36 Å (armchair direction) × 63.96 Å (zigzag direction) (contains 5,194 carbon atoms) onto an Fe NW with radius of 8.6 Å. The GNS is placed vertically to the axis of Fe NW and the attractive force between them makes the GNS approach to the Fe NW rapidly. The GNS displays discontinuous wrinkles or corrugations in several nanometers thick, showing its thermodynamic instability. According to the so-called Mermin-Wagner theorem (Mermin 1968), long-wavelength fluctuations destroy the long-range order of 2D crystals, and these fluctuations can be suppressed by anharmonic coupling between bending and stretching modes, which presents that a 2D GNS can exist but exhibit strong fluctuations with some ripples and corrugations (Fasolino et al. 2007). After the GNS attaching onto the Fe NW, the GNS begins to curl and quickly wrap around the Fe NW to form a coiling with a tail just like a tadpole (at $t = 15$ ps). When it totally wraps the Fe NW, the GNS begins to scroll spontaneously. At $t = 25$ ps, it is found that the tadpole-like part starts to fold and slide with a lower speed. Eventually, the self-scrolling completes and the configuration of GNS transforms from a planar membrane to a tubular scroll. During the self-scrolling, the speed is determined by the rate of releasing potential energy into the kinetic energy. Our simulation result indicates that the average self-scrolling speed of the GNS reaches up to 3.16 Å/ps (316 m/s). Interestingly, the Fe NW is also found to be deformed owing to the strong interaction between GNS and Fe NW during the self-scrolling process.

The spontaneous self-scrolling of a GNS onto an Fe NW leads to the structural transition of the GNS from a 2D to a 3D phase, and this process is irreversible no

matter whether the core-shell structure is cooled or heated to any temperature. The irreversibility of the structural transition clearly shows that the 2D structure of GNS is not the lowest energy configuration but is a metastable state like a supercooled liquid. We would expect a similar behavior of a GNS using metallic NWs of other elements and hope this distinctive property of metastable 2D GNS can bring more applications. Moreover, the multilayered scroll formed is very similar to multi-walled CNTs encapsulating with an Fe NW. Our results also demonstrate that such self-scrolling is a common phenomenon when the GNS adheres to other metallic NWs such as Cu, Au, Ag, Ge, and Sn. On the one hand, it would be a lot better to trigger the self-scrolling of a GNS onto a metallic NW in a controlled manner to produce metal/carbon core-shell nanostructures instead of the insertion of metallic particles into CNTs because it is extremely difficult to insert metals into the CNTs, which requires the conditions of the high temperature, catalyst, or other external energy (Li et al. 2007, 2006; Blank et al. 2010) due to the wetting and small size effect. This would provide a new method to prepare future nanoscale structures with a higher level of sophistication. The self-scrolling of GNS onto the metallic NW is also helpful for preventing the NW from oxidation when exposed to air.

1.3.2.2 Interface Characteristics

The interaction energy reflects the adhesion intensity between the GNS and the Fe NW which can be calculated from the following equation:

$$E_{\text{interaction}} = E_{\text{total}} - (E_{\text{GNS}} + E_{\text{NW}}), \tag{1.2}$$

where E_{total} is the potential energy of the system, E_{GNS} is the intrinsic energy of the single GNS without Fe NW, and E_{NW} is the energy of the single Fe NW without GNS.

Figure 1.12a shows the interaction energy between the GNS and the Fe NW during the self-scrolling. As the simulation continues, the interaction energy shows a rapid increase during the attaching process from $t = 0$ to 1.5 ps. From $t = 1.5$ to 15 ps, the interaction energy increases linearly with the increase of the contact area until the GNS just coils around the Fe NW. In order to further study the interaction between transitional Fe and sp^2 carbon on the GNS, DFT calculation has been performed. Figure 1.12b shows that the Fe atom is located above the center of the carbon hexagon on GNS with hollow H-site to form six covalent-like bonds with small adsorption energy of 0.96 eV. The bond length between Fe and the neighboring carbon is 2.14 Å, and the distance between Fe and GNS is 1.58 Å. We also computed the energy barrier for Fe migration in GNS from one H-site to its neighboring one. Figure 1.12c shows that some bonds break and Fe atom locates at the bridge B-site during the migration. The rather small migration energy barrier (0.66 eV) indicates that the H-site Fe atom can easily migrate on pristine GNS. Because the chemical energy between GNS and Fe NW is very weak, the covalent-like bonds do not affect the spontaneous scrolling of GNS onto Fe NW.
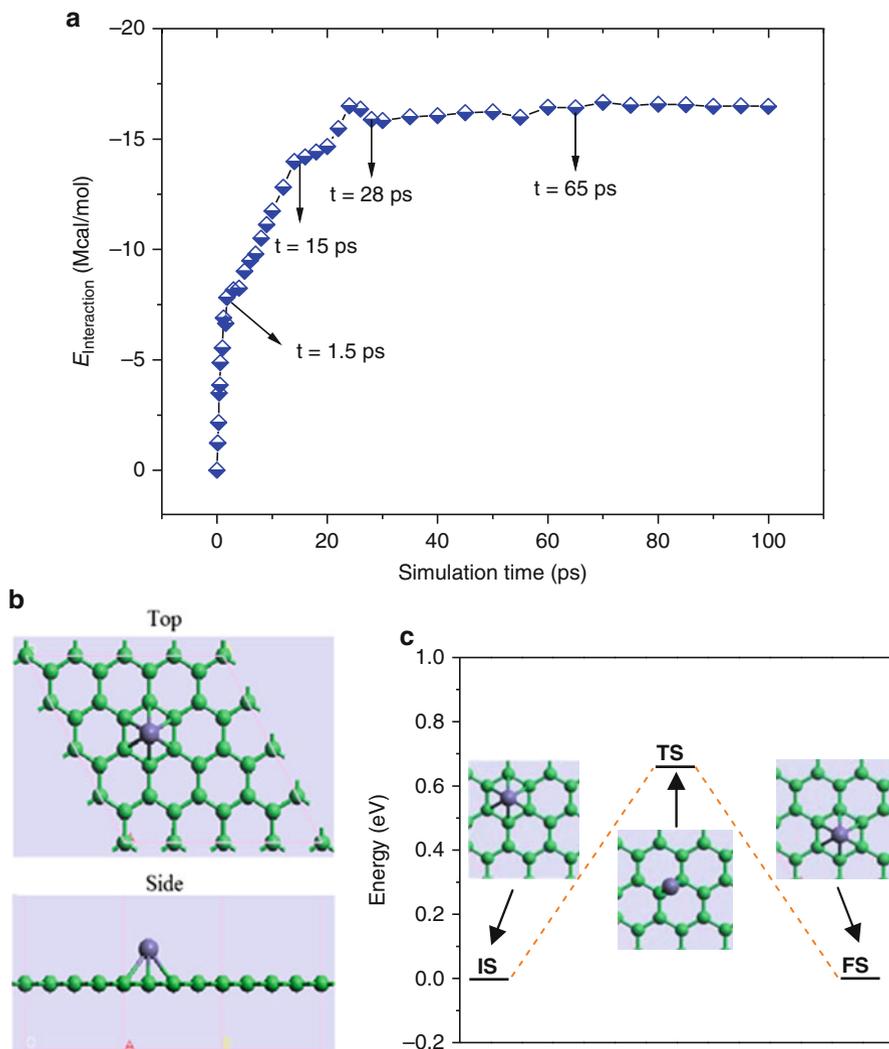
Fig. 1.12 (**a**) The interaction energy between GNS and Fe NW with time. (**b**) *Top* and *side* views of the geometric structures of Fe absorbed GNS calculated by DFT. (**c**) Energy profile for Fe diffusion on GNS from one H-site to its neighboring one; the *insets* are the initial state (*IS*), transition state (*TS*), and final state (*FS*)

From $t = 15$ ps, the increasing rate of interaction energy is much lower because the distance between the unwrapped GNS and the Fe NW increases with the increase of the scroll layer. It suggests that the interaction energy should be mainly determined by the contact area between the GNS layer and the Fe NW. From $t = 28$ ps (the sliding process), the interaction energy becomes almost unchanged until $t = 65$ ps
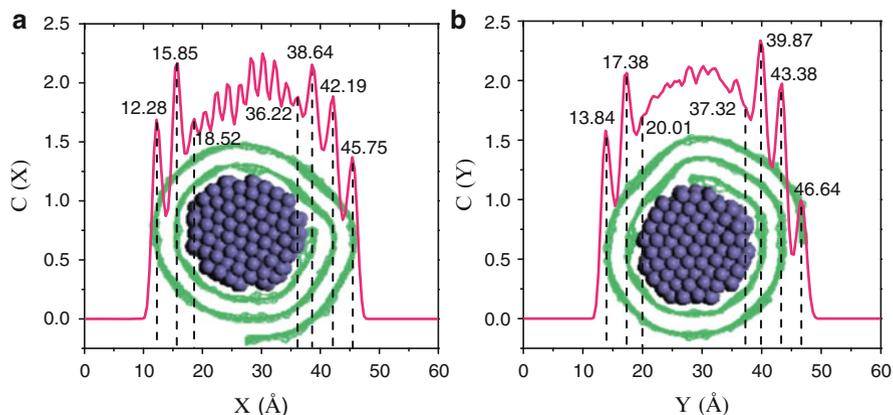
Fig. 1.13 Concentration profiles of the final structure in the X direction (**a**) and the Y direction (**b**). The *insets* are the snapshots of the core-shell structures and peak values

which indicates that the structural transition of the GNS has completed and the system reaches the equilibrium state. Therefore, we suggest that the structural transition of the GNS is maintained not only by the interaction between the GNS and the Fe NW but also by the interaction between the scrolled and unwrapped GNS layer.

The final structure can be further characterized by the concentration profile. Figure 1.13 shows the concentration profiles of the final structure consisting of the Fe NW and the GNS scroll in the X and Y directions. The separation of the adjacent layers can be obtained from the distance between two neighboring peaks in the concentration profiles. From the peak details marked in the inserts, on the one hand, the average separation distance between the innermost layer of the scroll and the Fe NW is 2.61 Å, bigger than that of DFT data. This difference may be due to distinct exchange and correlation functions used. However, this value is very close to the scale of the chemical bonding, still indicating that the interaction between them is very strong. On the other hand, the distance between the scrolled layers is about 3.52 Å, which is very close to the wall thickness of the multi-walled CNTs (3.4 Å), meaning this distance is in the strong-adhesive-binding region. In addition, the interaction energy between the GNS and the Fe NW reaches up to -16.5 Mcal/mol, suggesting that the adhesion is so strong that it is hard to strip the GNS off the Fe NW to recover its planar structure again.

1.3.2.3 The Mechanism

What we are concerned with is what causes the structural transition of the GNS from 2D to 3D phase. In principle, an isolated GNS can only lower its energy by bending to form corrugation to keep its 2D flat structure. The transition of an isolated, flat

Fig. 1.14 The evolutions of total potential energy E_P (**a**) and vdW energy E_{vdW} (**b**) versus time. The *insets* are the enlarge images of these two energies from $t = 0$ to 4 ps and snapshots at $t = 24$ ps
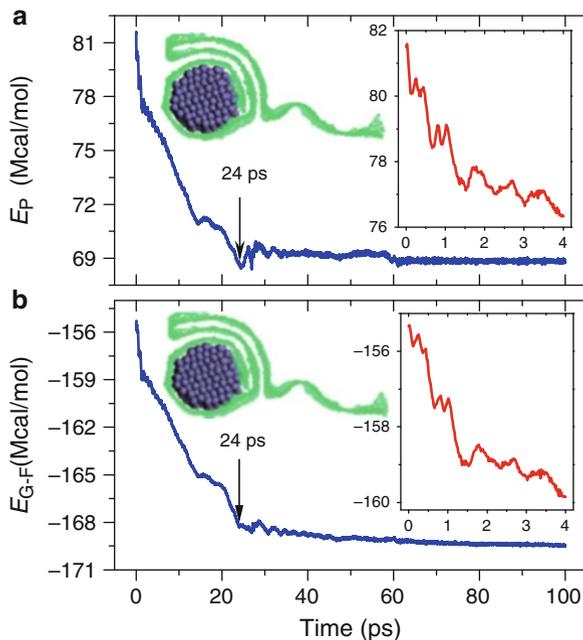
GNS membrane into a smaller, folded package is problematic because the intrinsic elastic energy of the GNS always tends to keep the GNS flat and generates energy barrier for the structural transition. When the Fe NW is introduced, the transition of GNS from a 2D planar membrane to a 3D scroll happens. It must be pointed out that there are two interaction effects responsible for this unique phenomenon. One interaction is the vdW interaction between GNS and Fe NW, which helps the GNS overcome the energy barrier and provides attractive force to drive the GNS to curl; the other one is the offset face-to-face π–π stacking interaction (Zhu et al. 2010) between GNS layers that causes the GNS continuously to hold tightly against the rolled surface to form scroll.

To reveal the effect of the vdW interaction between GNS and Fe NW on the structural transition of GNS, the evolutions of total potential energy E_P (a) and vdW energy ΔE_{vdW} (b) of the whole system versus time were tracked, as shown in Fig. 1.14. The inserts are enlarged images of two energies from $t = 0$ to 4 ps. The decrease of total potential energy of the system indicates that the spontaneous self-scrolling of GNS is a process of energy decreasing in which the system gradually reaches to a more stable state. During the structural transition, the evolutions of the vdW energy and the potential energy are nearly synchronous. The vdW energy is converted into kinetic energy partially, which sustains the structural transition. So we suggest that the interaction between GNS and Fe NW offers the main driving force to drive the structural transition, which keeps the GNS continuously moving toward and scrolling onto the Fe NW. It is worthy of note that, only from $t = 0$ to 24 ps

(the insets are the snapshots at $t = 24$ ps), both the potential energy and vdW energy have a rapid decrease. Thereafter, the potential energy reaches a minimum and remains almost unchanged, which indicates that the system has reached the most stable state from the suggestion of thermodynamics. Moreover, at 24 ps later, the release of the vdW energy becomes very slow, but the structural transition of the GNS still continues, suggesting that the vdW interaction between GNS and Fe NW only controls the former stage rather than the later one. The subsequent structural transition of the GNS is mainly determined by another interaction: the offset face-to-face π–π stacking interaction between GNS layers (Zhu et al. 2010; Nagy et al. 2003), resulted from an intermolecular interaction in the paralleled six-membered rings, which sustains the structural transition to form a multi-walled scroll in the end.

The offset face-to-face π–π stacking interaction has two sub-interactions, one is the π–π electron interaction and the other one is the π–σ interaction. The π–π electron interaction is an important repulsive force, which is roughly proportional to the area of π-overlap of the two six-membered rings. The π–σ interaction is an attractive force between π electrons of one ring and the σ-framework around the inner edge of the cavity of the other one. Different from π–π electron interaction, π–σ interaction can be maximized in displaced stacking. Furthermore, in a stacking system, stacked molecules should be exactly parallel with a vdW distance of about 3.5 Å (for the carbon skeleton) and overlapping at least partially to minimize repulsive interaction and maximize the attractive interaction of the π-system. Therefore, the best way to keep the displaced stacking and perfect parallel in GNS is that the arrangement of the GNS follows a scroll mode around the Fe NW when the GNS is self-scrolling onto the Fe NW. In the scroll, the paralleled six-membered system, displacement of the carbon rings favors minimization of repulsive π–π interaction and maximization of attractive π–σ interaction. To some extent, the high flexibility dependent on the perfect hexagonal honeycomb architectures and the intrinsic instability of the GNS has also contributed to the formation of the GNS scroll during the structural transition. Our simulation result just illustrates that the distances between the scrolled layers are exactly close to 3.5 Å, which accords well with the stacking distance of the offset face-to-face π–π stacking interaction (Główbka et al. 1999; Hunter and Sanders 2009; Yang et al. 2008). It indicates that the π–π stacking interaction plays a dominant role in the latter "scroll-forming" stage of the structural transition.

1.3.2.4 The Thermodynamic Model

To develop a thermodynamic model to further illustrate the nature of the structural transition of the GNS, we consider a GNS with length L and width W rolled onto a Fe NW with radius r_0. Thermodynamically, the occurrence of the structural transition of GNS is determined by the competition between the GNS-Fe binding energy, $E_{G-F} = -\sigma_{G-F}A_{G-F}$, and the GNS intrinsic elastic bending energy, $E_G = \sigma_G A_G$, where σ is the density of the binding energy and A is the binding area. The GNS-Fe (GNS-GNS) binding energies E_{G-F} (E_G) are easily obtained from the difference of the total

vdW energy of the system at two different states: One state is the distance between GNS and Fe NW is in their normal binding length, and the other one is the Fe NW is separated from the GNS by a very long distance. Scrolling of the GNS onto Fe NW is driven by the decrease of the GNS-Fe binding energy, $E_{\text{G-F}} = -\sigma_{\text{G-F}} A_{\text{G-F}}$. In the case as shown in Fig. 1.11, the GNS-Fe density of the binding energy is estimated as $\sigma_{\text{G-F}} \approx 2.388$ kcal/(mol·Å^2). When the GNS scrolls into a single-layered cylinder (at $t = 15$ ps), the initial and final GNS-Fe binding areas are $A_{\text{G-F}}^{\text{ini}} \to 0$ and $A_{\text{G-F}}^{\text{end}} = 2\pi \, (8.6 + 2.6) \times 63.96$ Å^2, respectively. The elastic binding energy of this GNS cylinder is $E_{\text{G}} = \sigma_{\text{G}} A_{\text{G}}$, where $A_{\text{G}} \approx A_{\text{G-F}}^{\text{end}}$ is the binding area. In order to obtain the strain energy density σ_{G} of the GNS cylinder, the flexural rigidity D of the pristine GNS is calculated firstly avoiding the effect of the Fe NW. To obtain the value of the parameter D, a pristine GNS with the size of $a \times b = 51.84 \times 31.98$ Å^2 is simulated, which is rolled into a cylinder with the radius of $R_0 = a/2\pi$. The σ_{e} is obtained by calculating the energy difference between the flat GNS and the cylinder. We obtain the value of $D = 25.6$ kcal/mol using $\sigma_{\text{e}} = (1/2) D \kappa^2$, where $\kappa = 1/R_0$ is valid in the linear elastic regime, which is in good agreement with ab initio result (Kudin and Scuseria 2001) and other model studies (Patra et al. 2009; Arroyo and Belytschko 2004), indicating that our study should be reasonable. Because $R_{\text{G}} \approx R_{\text{NW}} + 2.6 = 11.2$ Å and $\kappa = 1/R_{\text{G}}$, the obtained $\sigma_{\text{G}} \approx 0.102$ kcal/(mol·Å^2) is far less than the calculated $\sigma_{\text{G-F}} \approx 2.388$ kcal/(mol·Å^2), meaning $\sigma_{\text{G-F}} > \sigma_{\text{G}}$. Because $A_{\text{G-F}} \approx A_{\text{G}}$ during the wrapping process of the GNS onto the Fe NW before $t = 15$ ps, we obtain the energy condition of the structural transition of the GNS activated by the Fe NW:

$$E_{\text{G-F}} + E_{\text{G}} < 0 \tag{1.3}$$

During the wrapping process, the structure would become more and more stable since $E_{\text{G-F}}$ decreases rapidly due to the increase of the $A_{\text{G-F}}$.

During the structural transition, the self-scrolling of GNS has the outer radius R, the interlayer spacing h, and the fixed inner core radius r_0. The scrolled part of the GNS can be described by the polar equation $r = r_0 + (h/2\pi)\theta$, and parameters L, R, r_0 and h meet the relation $\pi \left(R^2 - r_0^2 \right) = xh$ approximately, where x denotes the length of the rolled GNS and $x \leq L$. The elastic energy per unit area of the scroll is taken to be $dQ(r)/dA = (1/2) D \times (1/r^2)$. Because of that $dA \approx Wr d\theta$ and $\theta = (r - r_0) 2\pi/h$, the total elastic energy in the scroll can be obtained as $Q = \pi DW/h \ln(R/r_0)$. When an infinitesimal length δx of the GNS is rolled, the outer radius R of the scroll would increase by $2\pi R \delta R = h \delta x$. Then the change of the strain energy is $\delta Q = (\pi DW/h) (\delta R/R) = DW \delta x \left/ \left[2 \left(xh/\pi + r_0^2 \right) \right] \right.$. The total surface energy of the scroll is altered by $\delta S = W(\gamma_{\text{CC}} + \gamma_{\text{CF}}) \delta x$, where γ_{CC} is the interlayer interaction energy per unit area of the GNS scroll and γ_{CF} is the interaction energy per unit area between the rolled GNS layer and Fe NW. Sum of the elastic energy and the surface energy is the total potential energy. Therefore, when displacement δx of GNS is rolled, the change of the total potential energy is $\delta V/\delta x = \delta Q/\delta x + \delta S/\delta x$. The releasing rate of the potential energy per unit area f is written as
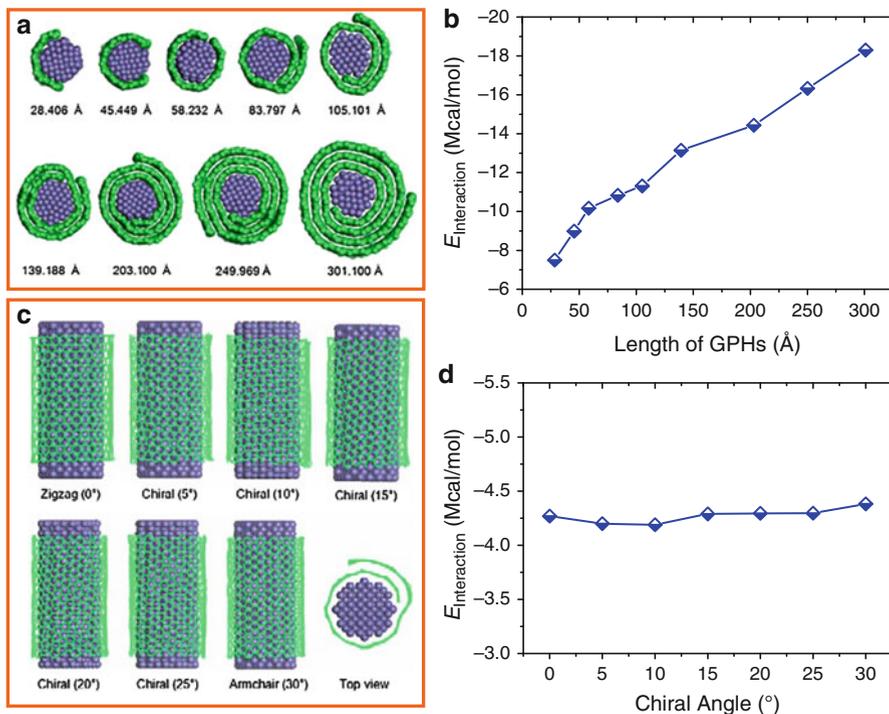
Fig. 1.15 (**a**) The self-scrolling of GNSs with different lengths onto the Fe NW with same radius 6.4 Å and (**b**) the saturation interaction energies. (**c**) Different chirality GNSs wrapping onto Fe NW exhibit different chiralities and (**d**) the saturation interaction energies

$$f = \frac{\delta V}{\delta x} \frac{1}{W} = \gamma_{CC} + \gamma_{CF} + \frac{D}{2\left(xh/\pi + r_0^2\right)} \tag{1.4}$$

which is the net driving energy of the continuous structural transition of the GNS. Given the initial condition and corresponding net driving energy, Eqs. (1.3) and (1.4) can be integrated to predict the structural transition of GNS activated by the Fe NW.

1.3.2.5 The Effect of Size, Chirality, and Position

We further studied the self-scrolling of nine GNSs with same width of 66.420 Å (zigzag direction) but different lengths of 28.406, 45.449, 58.232, 83.797, 105.101, 139.188, 203.100, 249.969, and 301.100 Å (armchair direction), respectively. Figure 1.15a illustrates that all GNSs are activated to completely self-scroll onto Fe NWs, forming arcs and single-layered or multi-shell structures with the Fe NW cores. Figure 1.15b shows the saturated interaction energy between the Fe NW and the GNS with different lengths. It can be seen that the interaction energy between the

GNS and the Fe NW rapidly increases until the length of the GNS reaches 58.232 Å, which corresponds to the length of the GNS that just completely wraps the NW with one circle. The final core-shell structure can be controlled by the radius of the Fe NW and the length of the GNS. If the length of the GNS L fit the equation

$$L = 2\pi \left(R_{NW} + d \right), \tag{1.5}$$

a perfect core-shell structure with single layer will be formed, where R_{NW} is the radius of the Fe NW and d is the average distance between the Fe NW and the GNS layer. When $L > 2\pi \left(R_{NW} + d \right)$, the GNS would overlap to form the multilayered scroll. If $L < 2\pi \left(R_{NW} + d \right)$, the GNS would paste onto the Fe NW to form an arc.

It is well known that the chirality has a significant effect on properties of GNSs, which can change their type from quasi-metallic to semiconducting (Jia et al. 2009). So it is essential to investigate the effect of the chirality on the structural transition. Figure 1.15c indicates that there are no obvious differences in their self-scrollings. Different kinds of scrolls exhibit different chiralities like CNT structures. To further clarify the effect of the chirality on the adhesion, Fig. 1.15d gives the saturation interaction energy between the Fe NW and the GNS with different chiralities. It shows that the chirality has a slight influence on the adhesion between the GNS and the Fe NW. Because the physical properties of the GNSs with different chiralities are different, we can produce different types of metal/GNS heterogeneous materials through this simple spontaneous scrolling, which are promising candidates for various applications including nanomechanical devices or nanocircuits.

The position of the Fe NW on GNS has a great effect on the self-scrolling. When the GNS length L and Fe NW radius R_{NW} meet the equation $L \leq 2\pi \left(R_{NW} + d \right)$, the GNS will paste to the NW no matter where the Fe NW is located as illustrated in Fig. 1.16a. However, when $L > 2\pi \left(R_{NW} + d \right)$, the self-scrolling of GNS would be greatly affected by the position of the Fe NW. In order to explore the position effect of the Fe NW, We study the self-scrolling of an armchair GNS with length 207.361 Å onto a Fe NW with radius 6.41 Å. Figure 1.16b illustrates the snapshots of the Fe NW located in different positions i, ii, iii, and iv. For the Fe NW with the radius of 6.41 Å, only the distance D between the Fe NW and one end of the GNS meets $D \leq 37.9$ Å; the GNS can wrap onto the Fe NW to form multilayered scroll. When $D > 37.9$ Å, though the structural transition is also activated, the GNS does not self-scroll onto the Fe NW to form multilayered scroll but a knot structure, as illustrated at positions iii and iv, respectively. Figure 1.16c shows snapshots of the typical structural transition activated by the Fe NW located at the middle. At $t = 1.5$ ps, the GNS starts to wrap onto the NW. After two sides of the GNS meet, they contact each other to create more contact area and then fold tightly in opposite directions, respectively. Two ends oscillate up and down and finally a knot structure with double shells forms.

Next, we will further clarify how the initial angle (φ) between the GNS and the Fe NW affects the self-scrolling. In Fig. 1.17a, the tip of a narrow GNR with size of 22.85×277.67 Å^2 is initially positioned on the Fe NW at the angle of $\varphi = 60°$ with
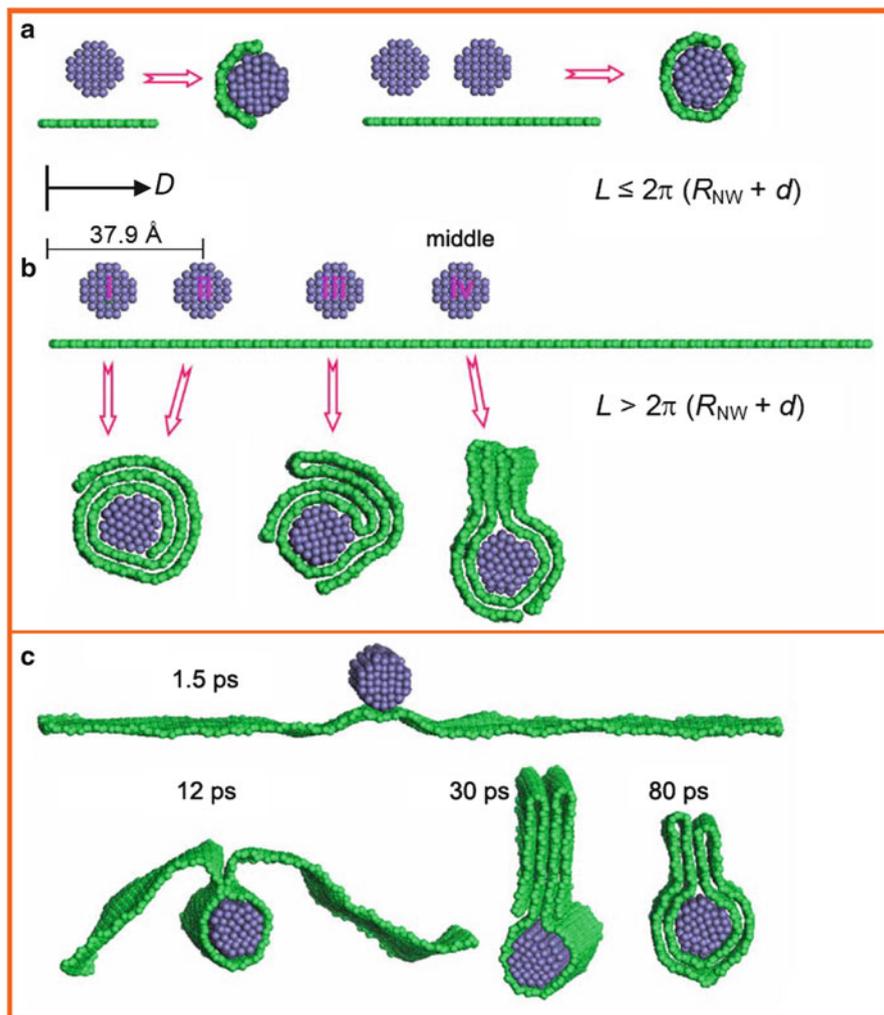
**Fig. 1.16** (**a**, **b**) Illustration of the position effect of the Fe NW on the self-scrolling of the GNS with different lengths and the final nanostructures. (**c**) A typical self-scrolling of the GNS onto the Fe NW located at the *middle*

respect to the axis of the Fe NW. The tip is attracted to the Fe NW fast and then move forward along the axial direction until the tip reaches another end of Fe NW. At $t = 30$ ps, the GNR starts to scroll around the Fe NW spirally with large pitch. Then the pitch becomes small, and GNR eventually forms a stable helix with the distance between the neighboring edges 3.5 Å. In this process, the GNS and Fe NW also satisfy the above-mentioned energy condition: $E_{G\text{-}F} + E_G < 0$, and the increase
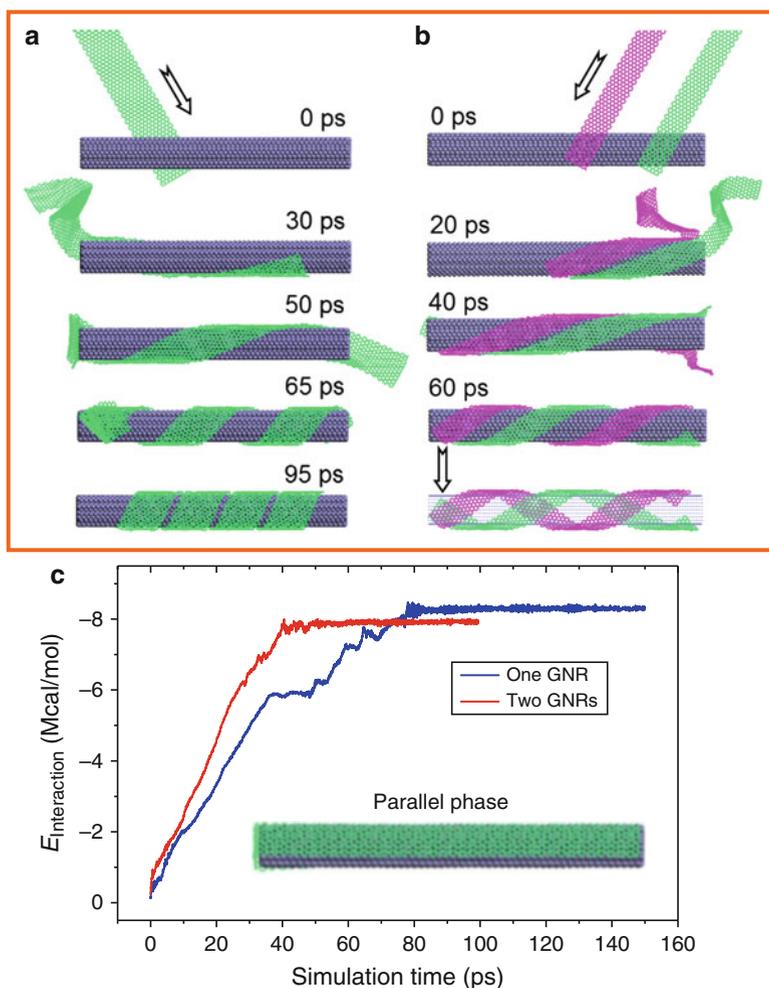
Fig. 1.17 Snapshots of the helical rolling of one (**a**) and two GNRs (**b**) when placed at the angle of $\varphi = 60°$ with respect to the axis of the Fe NW. (**c**) The interaction energies between GNS and Fe NW during these two structural transition processes. The *inset* in (**c**) is the parallel phase of GNR on Fe NW

of the contact area enhances the stability of the whole system. We further study the spontaneous wrapping of two GNRs (183.93×14.76 Å^2) with initial angle $\varphi = 60°$ on the Fe NW, as shown in Fig. 1.17b. As simulation begins, two GNRs start to move forward side by side on the Fe NW. At $t = 20$ ps, they start to fold helically in the same direction. Finally, they form a loose double helix with large pitch, which

closely resembles to the double-stranded DNA. The interaction energy between the Fe NW and GNR during the scrolling is shown in Fig. 1.17c. In two cases, the interaction energy between them increases linearly with the increase of the contact area until the GNRs fully wrap the Fe NWs. It verifies the fact that the interaction energy is mainly determined by the contact area between the GNS and Fe NW. Our simulations further reveal that if the initial angle is small, the thin GNR does not wrap spirally but adhere on the Fe NW parallel (parallel phase), as seen the inset in Fig. 1.17c. The above results indicate that the self-scrolling and final configuration of GNS can be controlled by the position, initial angle, and GNS width.

In the above discussion, we mainly focused on the self-scrolling of the GNS onto the NW that is long enough to form the core-shell structure. In order to determine whether there exists a critical length of NW, below which the perfect self-scrolling (as shown in Fig. 1.11) of GNS will not operable, the interaction between a GNS (83.80×83.797 Å^2) and a series of Fe NWs with different lengths and same radius (8.6 Å) is further studied. From our calculations, the length of Fe NW (L_{NW}), ensuring the perfect self-scrolling of GNS, should be longer than the critical value $W_{GNS}/2$ ($L_{NW} \geq W_{GNS}/2$), where W_{GNS} is the width of GNS parallel aligned with the NW. Otherwise, the GNS will fold onto Fe NW to form knot or dumpling-like structures. However, when the Fe NW is a bit shorter than the critical value, the perfect core-shell structure will still be formed if the GNR can well self-adjust, but it is much more difficult and uncertain.

1.3.2.6 Possible Applications

The unique self-scrolling properties of the GNS arouse our interest to utilize it as nanoscale conveyor belt to deliver substances to the surface of Fe NW for modification. Recent experiment showed that the NW modified by the aminothiol molecule can be used to deliver plasmid DNA into different cells (Kuo et al. 2008). To explore the possible application, some butyl aminothiol molecules are chemically attached to the GNS uniformly. Just as shown in Fig. 1.18, the GNSs modified by aminothiol molecules can spontaneously wrap the Fe NWs and form the scroll and helix. The attached molecules have a little influence on the structural transition and the final structure. Besides the aminothiol, other molecules such as drugs, catalysts, and enzymes can also be attached to the GNS and easily carried onto the Fe NW. The amount of the modified molecules can be easily managed and located at the specified position on a given Fe NW, since the distance between the NW and the GNS and that of the neighboring segments in GNS helix is easily known. Then the functional molecules can be distributed according to the individual requirement. Hence, the GNS can be a promising nanoscale conveyor belt to deliver molecules to modify the metallic NWs to develop their probing to the biological and medical systems.
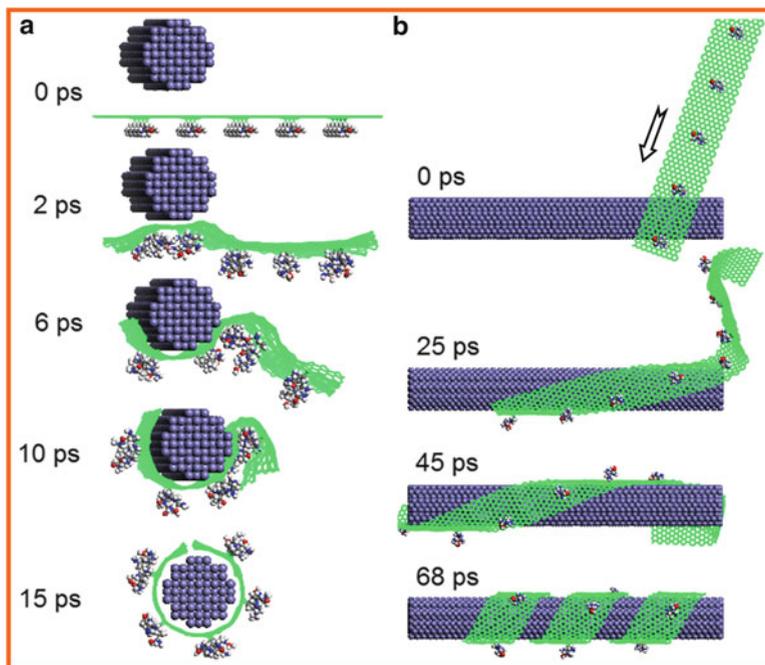
Fig. 1.18 Snapshots of the aminothiol-modified GNS (**a**) and GNR (**b**) gradually wrapping onto Fe NWs

1.4 Dynamic Ripples Reduced by the Impact of a C60 Molecule in Single-Layer Graphene

Recently, it has been found that a freestanding isolated graphene layer can be intrinsically corrugated to produce ripples, which are expected to affect its conductivity (Meyer et al. 2007b). Another approach to create periodic ripples into graphene has been reported by Bao and colleagues by utilizing the negative expansion coefficient of graphene sheet (Bao et al. 2009). The formation of ripple, which is related to the periodic variation of electronic properties of graphene, is expected to be used for synthesizing graphene-based electronic devices (Miranda and Vázquez de Parga 2009).

Here, we report an MD simulation of ripple formation and propagation in a single-layer graphene (SLG), induced by the impact of a C60 molecule. To mimic the classical single- or double-slit experiments, we also demonstrate the diffraction and interference of ripples in graphene.
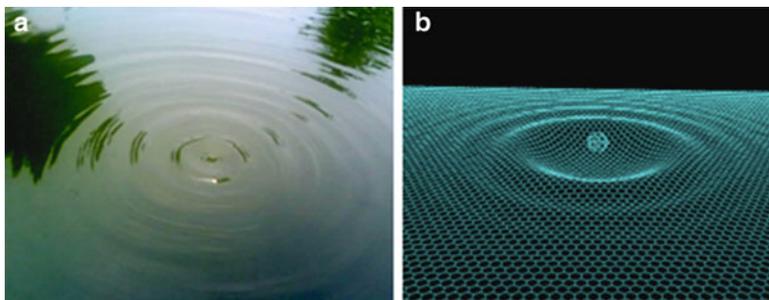
Fig. 1.19 Snapshots of water wave and graphene ripple. (**a**) Water waves are generated by means of throwing a pebble to the static water pond (Nikon coolpix L22). (**b**) Graphene ripples are generated on the graphene which is stroked by an energic C60 molecule

1.4.1 Simulation Method

In this MD simulation, the second-generation reactive empirical bond order (REBO) potential is used to describe the C–C interaction (Brenner et al. 2002; Li et al. 2009c), and the Lennard-Jones 12-6 potential is used to calculate the long-range van der Waals interaction. It is important to note that the ultrathin 2D graphene sheet is the medium of ripple propagation. Graphenes of two different sizes are studied. One graphene sheet has a size of 197 Å (zigzag direction) × 169 Å (armchair direction) (containing 12,880 atoms). The size of another is 254 Å (armchair direction) × 153 Å (zigzag direction) (containing 14,040 atoms). In order to observe the wave diffraction and interference, two symmetrical slits with a width of 3 Å are created along a centerline of the latter graphene (all C atoms on the centerline, except those that belong to the slits, are fixed during the simulation). Initially, a C60 molecule is placed 6.5 Å above the graphene. At time zero, the C60 starts to impact the SLG with an initial vertical velocity of 15 Å/ps. The time step of the MD simulation is 1 fs and each trajectory runs for 10 ps.

1.4.2 Results and Discussion

A snapshot of circular ripples propagating in the SLG during the simulation is shown in Fig. 1.19b. It is interesting that these circular ripples are very similar to the water waves stirred by dropping a pebble into a pond (Fig. 1.19a). Different from the water wave in a pond, the ripple in SLG is arisen by distortion of C–C bonds. As vibration energy is passing through the graphene from the impacting center to another place, the ripples are formed. The ripple propagation in the SLG actually means that the "strong" impact energy is transformed into the "soft" wave energy, illustrating that the graphene can be used as an energy buffer to withstand shocks.
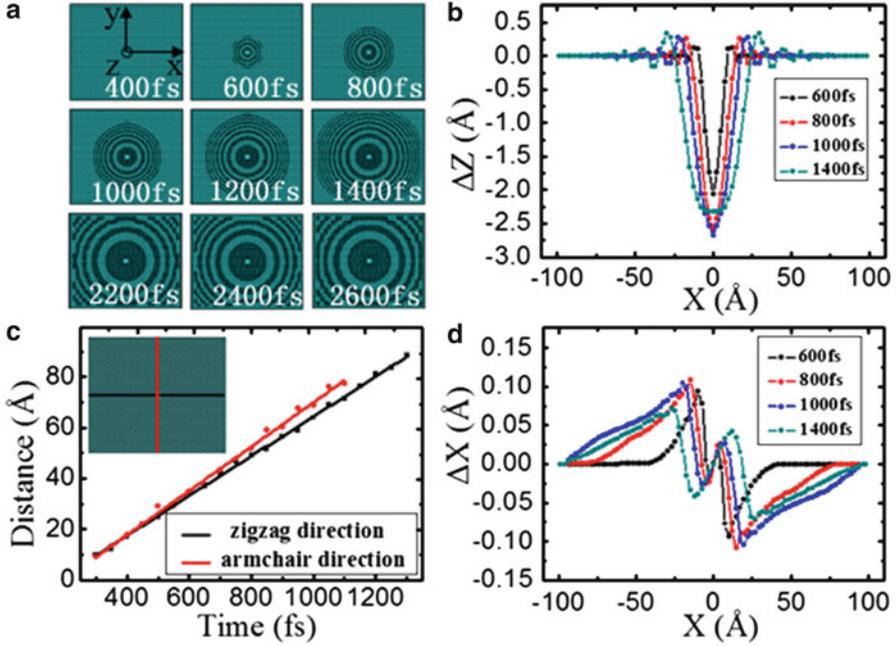
Fig. 1.20 (**a**) The onset of the graphene ripple generated by striking with C60 molecule and its propagation on the surface of the graphene. The original ripples and the reflective ripples arouse interference pattern in the last three snapshots. (**b**) and (**d**) show the Z direction displacements (Δz) and X direction displacements (Δx) of atoms along the centerline [*colored black* in (**c**)], respectively. (**c**) The travelling distance of the ripples along different directions

The onset of the graphene ripple and its propagation in the SLG are demonstrated in Fig. 1.20a. The Z direction displacements (Δz) of atoms on the centerline versus time curves Fig. 1.20b are used to illustrate the transverse waves. At 800 fs, the displacement of the atoms at the impacting point is about 2.6 Å. The amplitude of the nearest wave crest of the impacting point is 0.26 Å. The amplitude of the wave decays as the following exponential function:

$$A(x) = 2.59943 \exp\left(-\left|x\right|/7.33993\right) - 0.01351, \tag{1.6}$$

where x (in angstrom) is the horizontal position and $A(x)$ (in angstrom) is the corresponding amplitude. The distances of ripple propagation at different times are shown in Fig. 1.20c. The average propagating speed of ripples along the zigzag direction is 78.32 Å/ps, while the propagating speed of ripples along the armchair direction is 87.02 Å/ps. The small difference between the two displacement lines results in a hexagonal symmetry of the ripples rather than complete circles (as shown in Fig. 1.20a). Meyer et al. mentioned that, under the condition of thermal equilibrium, ripples in freestanding graphene are intrinsic, random, and
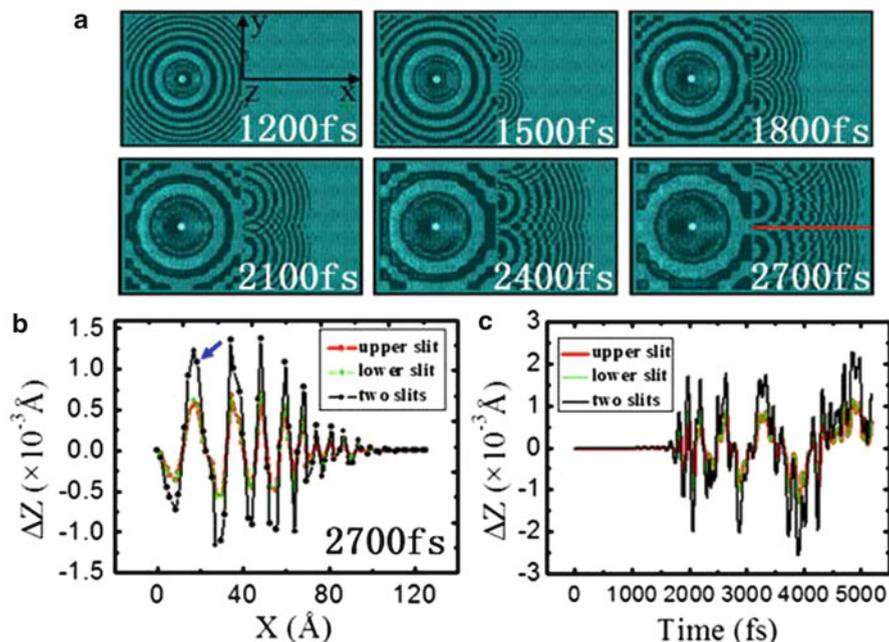
Fig. 1.21 (**a**) Snapshots of interference of ripples coming from two slits. (**b**) The Z direction displacements (Δz) of atoms on the centerline [*colored red* in (**a**)]. (**c**) The Z direction displacements of the atom pointed by a *blue arrow* in (**b**) at different times. The *red line* and *green line* indicate the displacement caused by the diffraction wave when the two slits are closed, respectively, while the *black line* indicates the displacement caused by the diffraction wave when the two slits are both open

uncontrollable (Meyer et al. 2007a, b). However, this study shows that, by C60 striking, the ripple forming on the surface of SLG is reproducible and controllable. For example, the amplitude of ripple can be easily tuned by varying the impacting speed of the C60.

The X direction displacements (Δx) of atoms along the centerline are shown in Fig. 1.20d. The atoms near the zero point do not move along the X direction. With the increase of distance from the impacting point, Δx fluctuates between positive and negative. By comparing Δx with Δz, it is found that the Z direction displacement of atoms is much larger than the X direction displacement. Graphene shrinks as any other 2D membranes due to transverse bending vibrations. Muñoz et al. (2010) discussed the ballistic heat conductivity of graphene and showed that the soft bending mode dominated the graphene thermal conductivity at low temperature. This is in agreement with our simulation that propagation of the transverse wave is free in the graphene, which means that the free path of bending mode phonons is very large.

When the ripples reach a narrow slit, the atoms in the slit vibrate like a point source. Noticeable diffraction is shown in Fig. 1.21a. The diffraction wave

resembles a circular ripple with the slit as its center. Our results indicate that this mechanical ripple can spread out along the narrow slit (one atom distance), which would provide a possible technique to detect defects in graphene. For example, if there is a vacancy defect in the graphene, the shape of ripple would be different due to the wave diffraction at the vacancy defect. When the ripple arrives at the vacancy point, the smooth circle ripple at the defect point would form a small crater or even be separated into two parts, which is dependent on the size and shape of the vacancy. If lots of vacancy defects exist, the circle ripple would become quite unsmooth with some concaves. Therefore, we can determine the existence of vacancy defect by observing the shape of ripple.

When the two diffraction waves encounter in the double-slit interference experiment, interference is generated (shown in Fig. 1.21a). Figure 1.21b shows the displacements of a string of atoms along the centerline at 2,700 fs. The two point sources of the diffraction waves are also bilaterally symmetrical due to two localized bilaterally symmetrical slits. When the two slits are closed, respectively, it is found that the two displacement curves would almost fully overlap. However, once the two slits are both open, the resultant displacement is equal to the sum of the above two displacements, which accords with the principle of superposition of waves. In this way, the vibrations of all the atoms along the centerline are strengthened. Then, a single atom is picked from the central row of atoms in order to study the change of displacement as a function of time (shown in Fig. 1.21c). It is found that the displacement-time curves of the single atom are also corresponded to the above superposition principle. The above phenomena indicate that ripples propagating in a 2D single-atom-thick media can produce interference. We can use this concept of "superposition of waves" to design a "lens" that focuses wave energy on the SLG sheet, which would open an exciting possibility of the fabrication of nanodevices (e.g., signal transducer).

The above-mentioned graphenes are perfect 2D crystals which are not stable according to both theory and experiment (Mermin 1968; Meyer et al. 2007a, b; Novoselov et al. 2005a, b). There should be intrinsic ripples at finite temperatures due to its thermodynamic stability. When a graphene with intrinsic ripples is stroked by a C60 molecule, ripples also exist at the impacting point and propagate outside as shown in Fig. 1.22. It is found that impacting ripples on the plane graphene are different from those on the corrugated graphene. On one hand, the intrinsic ripples would inevitably affect the impacting ripples. The bending and stretching of the graphene layer result in the intrinsic ripples which are distributed randomly and uncontrollably. Therefore, the graphene surface is no longer plane and symmetric. During the propagating process, the impacting ripples vary with the different directions. On the other hand, the impacting ripples would affect the intrinsic ripples in turn. The propagation of impacting ripples breaks the original stability of graphene and thus changes the intrinsic ripples. As shown in Fig. 1.22, there are many cloudlike shades outside the impacting ripples, which mean that the amplitudes of intrinsic ripples in these areas have decreased. When the impacting ripples arrive at a slit, diffraction still occurs and brings cloudlike shades. However, interference of diffraction ripples coming from the two slits is
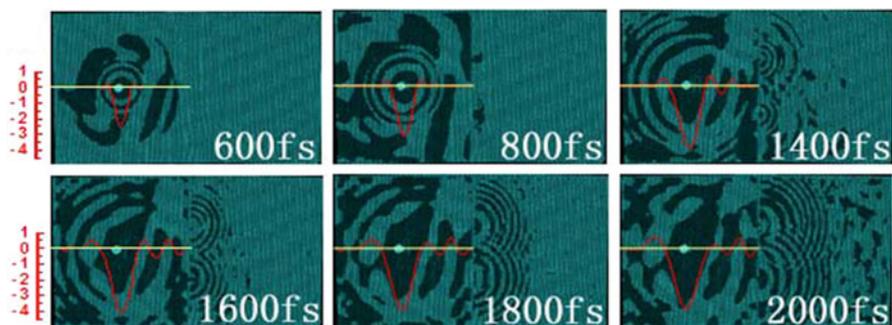
Fig. 1.22 The propagation, diffraction, and interference of impacting ripples in the corrugated graphene. The inset *red line* of each graph is the Z direction displacements of atoms on the *yellow line*. Tick labels on the *left* are in unit of angstrom

not as clear as that of plane graphene. Although the intrinsic ripples disturb the impacting ripples, the signal carried by the impacting ripples does not fade away but still propagates forward. Intrinsic ripples in graphene are expected to strongly influence its electronic properties by introducing spatially varying potentials or effective magnetic fields (Park et al. 2008; Castro Neto et al. 2009). Different from intrinsic ripples, the impacting ripples made from C60 will disappear after the system is fully relaxed. However, the impacting ripple has its own excellent feature such as reducing local excessive deformation, transferring signals caused by striking, and detecting cracks or defects.

1.5 Conclusion

A series of atomistic MD simulations has been conducted to explore the interaction and the structural properties of GNR-SWNT and GNS-NW systems. The GNRs can helically wrap and insert the SWNT spontaneously to form helical configurations, which are quite close to the helices found in nature. The steady decline of the potential energy in the GNR-SWNT system suggests that the helical wrapping and insertion are spontaneous phenomena and systems are increasingly stable during these two processes. The vdW attraction drives the GNR continuously moving toward the tube and traps the GNR to adhere on the sidewalls of tubes, whereas the formation of the GNR helix is attributed to the $\pi-\pi$ stacking interaction between GNR and SWNT as well as the dangling σ-orbitals on carbon atoms at the open edges of GNR. A DNA-like double helix with same handedness would be formed with the wrapping and insertion of two GNRs. The velocity of GNR in helical wrapping is obviously lower than that in helical insertion. The diameter and chirality of tube have a neglect influence on the wrapping, whereas the encapsulation is limited by the diameter greatly.

Moreover, the GNSs can spontaneously self-scroll onto the Fe NWs irreversibly, which results in the structural transition of the GNS from 2D to 3D phase and the formation of the stable metal/carbon core-shell nanostructure. The planar GNS is in metastable state, just like the supercooled liquid. The interaction between the GNS and Fe NW as well as the π–π stacking interaction between GNS layers may be responsible for this unique phenomenon. The decline of the potential energy of the whole system suggests that the self-scrolling of the GNS onto Fe NW is spontaneous, and the system is increasingly stable during this process. A thermodynamic model has been proposed to explain and predict the structural transition of GNS. The final core-shell nanostructure can be controlled by the positions of GNS and Fe NW.

MD simulation results also show that impact of C60 molecule would induce nanoscale dynamic ripples on the graphene no matter whether the graphene is plane or corrugated, although there are lots of differences between them. A GNS may be a well-promising material to be served as an energy buffer to withstand shocks. The propagation orientation and amplitude of ripples can be controlled via changing the locally insert slits and the speed of C60. The graphene ripple is a kind of surface wave which carries a lot of surface information, and the wave energy could also be focused due to the interference of ripples. The controlled ripples and their diffraction and interference in graphene are of great significance to detect the cracks and defects in the graphene sheet by receiving the wave signals.

This study provides possible applications for the GNS and GNR to serve as conveyor belt for molecule delivery. And also, the discoveries of this study are of great significance for the deeper understanding of the instability and properties of graphene at an atomic level and the further exploration of the properties of the GNR-SWNT and GNS-NW systems.

References

Arroyo M, Belytschko T (2004) Phys Rev B 69:115411
Bao W, Miao F, Chen Z, Zhang H, Jang W, Dames C, Lau CN (2009) Nat Nanotechnol 4:562
Baskaran D, Mays JW, Bratcher MS (2005) Chem Mater 17:3389
Bets KV, Yakobson BI (2009) Nano Res 2:161
Blank VD, Kulnitskiy BA, Perezhogin IA, Polyakov EV, Batov DV (2010) Acta Mater 58:1293
Borissov D, Isik-Uppenkamp S, Rohwerder M (2009) J Phys Chem C 113:3133
Brenner DW, Shenderova OA, Harrison JA, Stuart SJ, Ni B, Sinnott SB (2002) J Phys Condens Matter 14:783
Bunte SW, Sun HJ (2000) Phys Chem B 104:2477
Castro Neto AH, Guinea F, Peres NMR, Novoselvo KS, Geim AK (2009) Rev Mod Phys 81:109

Chen RJ, Zhang Y, Wang D, Dai H (2001) J Am Chem Soc 123:3838
Choi WY, Kang JW, Hwang HJ (2003) Phys Rev B 68:193405
Demoncy N, Stephan O, Brun B, Collix C, Loiseau A, Pascard H (1998) Eur Phys J B 4:147
Fasolino A, Los JH, Katsnelson MI (2007) Nat Mater 6:858
Fujii S, Enoki T (2010) J Am Chem Soc 132:10034
Gao H, Kong Y, Cui D, Ozkan CS (2003) Nano Lett 3:471
Gao XP, Zhang Y, Chen X, Pan GL, Yan J, Wu F, Yuan HT, Song DY (2004) Carbon 42:47
Głóbwka ML, Martynowski D, Kozłowska K (1999) J Mol Struct 474:81
Goswami S, Maiti UN, Maiti S, Nandy S, Mitra MK, Chattopadhyay KK (2011) Carbon 49:2245
Govind N, Petersen M, Gitzgerald G, King-Smith D, Andzelm J (2003) J Comput Mater Sci 28:250
Gulseren O, Ercolessi F, Tosatti E (1998) Phys Rev Lett 80:3775
He YZ, Li H, Si PC, Li YF, Yu HQ, Zhang XQ, Ding F, Liew KM, Liu XF (2011) Appl Phys Lett 98:063101
Hilder TA, Hill JM (2009) Small 5:300
Hong B, Bae S, Lee CW, Jeong S, Kim K (2001) Science 294:348
Hunter CA, Sanders JKM (2009) J Am Chem Soc 112:5525
Jia XT, Hofmann M, Meunier V, Sumpter BG, Campos-Delgado J, Romo-Herrera JM, Son H, Hsieh Y, Reina A, Kong J, Terrones M, Dresselhaus MS (2009) Science 323:1701
Jiang YY, Li H, Li YF, Yu HQ, Liew KM, He YZ, Liu XF (2011) ACS Nano 5:2126
Juang ZY, Wu CY, Lu AY, Su CY, Leou KC, Chen FR, Tsai CH (2010) Carbon 48:3169
Kalbacova M, Broz A, Kong J, Kalbac M (2010) Carbon 48:4323
Khan U, Ryan K, Blau WJ, Coleman JN (2007) Compos Sci Technol 67:3158
Kim KS, Zhao Y, Jang H, Lee SY, Kim JM, Kim KS, Ahn J-H, Kim P, Choi JC, Hong BH (2009) Nature 457:706
Kondo Y, Takayanagi K (1997) Phys Rev Lett 79:3455
Kondo Y, Takayanagi K (2000) Science 289:606
Kudin KN, Scuseria EG (2001) Phys Rev B 64:235406
Kuo CW, Lai JJ, Wei KH, Chen PL (2008) Nanotechnology 19:025103
Ledoussal P, Radzihovsky L (1992) Phys Rev Lett 69:1209
Li YF, Hatakeyama R, Kaneko T, Izumida T, Okada T, Kato T (2006) Appl Phys Lett 89:093110
Li YF, Hatakeyama R, Shishido J, Kato T, Kaneko T (2007) Appl Phys Lett 90:173123
Li H, Li YF, Liew KM, Zhang JX, Liu XF, Fan RH (2009a) Appl Phys Lett 95:063106
Li H, Li YF, Liew KM, Zhang JX, Liu XF (2009b) Appl Phys Lett 95:183101
Li H, Sun FW, Liew KM, Liu XF (2009c) Scr Mater 60:129
Li H, Knaup JM, Kaxiras E, Vlassak JJ (2011a) Acta Mater 59:44
Li YF, Sun FW, Li H (2011b) J Phys Chem C 115:18459
Li YF, Yu HQ, Li H, An CG, Zhang K, Liew KM, Liu XF (2011c) J Phys Chem C 115:6229
Li YF, Li H, Zhang K, Liew KM (2012) Carbon 50:566
Mermin ND (1968) Phys Rev 176:250
Meyer JC, Geim AK, Katsnelson MI, Novoselov KS, Obergfell D, Roth S, Girit C, Zettl A (2007a) Solid State Commun 143:101
Meyer JC, Geim AK, Katsnelson MI, Novoselov KS, Booth TJ, Roth S (2007b) Nature 446:60
Miranda R, Vázquez de Parga AL (2009) Nat Nanotechnol 4:549
Mohaddes-Ardabili L, Zheng H, Ogale SB, Hannoyer B, Tian W, Wang J, Lofland SE, Shinde SR, Zhao T, Jia Y, Salamanca-Riba L, Schlom DG, Wuttig M, Ramesh R (2004) Nat Mater 3:533
Muñoz E, Lu J, Yakobson BI (2010) Nano Lett 10:1652
Nagy PI, Alagona G, Ghio C, Takács-Novák K (2003) J Am Chem Soc 125:2770
Naito M, Nobusawa K, Onouchi H, Nakamura M, Yasui K, Ikeda A, Fujiki M (2008) J Am Chem Soc 130:16697
Nish A, Hwang JY, Doig J, Nicholas RJ (2007) Nat Nanotechnol 2:640
Novoselov KS, Geim AK, Morozov SV, Jiang D, Zhang Y, Dubonos SV, Grigorieva IV, Firsov AA (2004) Science 306:666
Novoselov KS, Geim AK, Morozov SV, Jiang D, Katsnelson MI, Grigorieva IV, Dubonos SV, Firsov AA (2005a) Nature 438:197

Novoselov KS, Jiang D, Schedin F, Booth TJ, Khotkevich VV, Morozov SV, Geim AK (2005b) Proc Natl Acad Sci USA 102:10451

Numata M, Asai M, Kaneko K, Bae AH, Hasegawa T, Sakurai K, Shinkai S (2005) J Am Chem Soc 127:5875

Ohiwa T (1976) Bot Mag 89:259

Opitz J, Zahn P, Mertig I (2002) Phys Rev B 66:245417

Park CH, Yang L, Son Y-W, Cohen ML, Louie SG (2008) Nat Phys 4:213

Patra N, Wang BY, Kral P (2009) Nano Lett 9:3766

Pederson MR, Broughton JQ (1992) Phys Rev Lett 69:2689

Perdew JP, Wang Y (1992) Phys Rev B 45:13244

Potts JR, Lee SH, Alam TM, An J, Stoller MD, Piner RD, Ruoff RS (2011) Carbon 49:2615

Prakash G, Capano MA, Bolen ML, Zemlyanov D, Reifenberger RG (2010) Carbon 48:2383

Sandoval L, Urbassek HM (2009) Nano Lett 9:2290

Savini G, Dappe YJ, Öberg S, Charlier JC, Katsnelson MI, Fasolino A (2011) Carbon 49:62

Seidel R, Mertig M, Pompe W (2002) Surf Interface Anal 33:151

Sen D, Novoselov KS, Reis PM, Buehler MJ (2010) Small 6:1108

Seol JH, Jo I, Moore AL, Lindsay L, Aitken ZH, Pettes MT, Li X, Yao Z, Huang R, Broido D, Mingo N, Ruoff RS, Shi L (2010) Science 328:213

Snir Y, Kamien RD (2005) Science 307:1067

Sorin EJ, Pande VS (2006) J Am Chem Soc 128:6316

Sulong AB, Muhamad M, Sahari J, Ramli R, Deros BM, Park J (2009) Eur J Sci Res 29:13

Sun H (1998) J Phys Chem B 102:7338

Svensson K, Olin H, Olsson E (2004) Phys Rev Lett 93:145901

Tasis D, Tagmatarchis N, Bianco A, Prato M (2006) Chem Rev 106:1105

Thurn-Albrecht T, Schotter J, Kstle G, Emley N, Shibauchi T, Krusin-Elbaum L, Guarini K, Black CT, Tuominen MT, Russell TP (2000) Science 290:2126

Wang B, Yin S, Wang G, Buldum A, Zhao J (2001) Phys Rev Lett 86:2046

Wang ZY, Li H, Liu Z, Shi ZJ, Lu J, Suenaga K, Joung SJ, Okazaki T, Gu ZN, Zhou J, Gao ZX, Li GP, Sanvito S, Wang E, Iijima S (2010) J Am Chem Soc 132:13840

Warner JH, Wilson M (2010) ACS Nano 4:4011

Xu ZP, Buehler MJ (2010) ACS Nano 4:3869

Yan KY, Xue QZ, Xia D, Chen HJ, Xie J, Dong MD (2009) ACS Nano 3:2235

Yang XY, Zhang ZY, Liu ZF, Ma YF, Huang Y, Chen YS (2008) J Phys Chem C 112:17554

Zhang Y, Dai HJ (2000) Appl Phys Lett 77:3015

Zhang GD, Kuntz JD, Wan J, Mukherjee AK (2003a) Nat Mater 2:38

Zhang XY, Wen GH, Chan YF, Zheng RK, Zhang XX, Wanga N (2003b) Appl Phys Lett 83:3341

Zheng QB, Geng Y, Wang SJ, Li ZG, Kim JK (2010) Carbon 48:4315

Zhou Z, Zhen J, Karpowich NK, Goetz RM, Law CJ, Reith MEA, Wang DN (2007) Science 317:1390

Zhu CZ, Guo SJ, Fang YX, Dong SJ (2010) ACS Nano 4:2429

Zorbas V, Ortiz-Acevedo A, Dalton AB, Yoshida MM, Dieckmann GR, Draper RK, Baughman RH, Jose-Yacaman M, Musselman IH (2004) J Am Chem Soc 126:7222

Chapter 2
First-Principles Study of the Electronic and Magnetic Properties of Defects in Carbon Nanostructures

Elton J.G. Santos, Andrés Ayuela, and Daniel Sánchez-Portal

Abstract Understanding the magnetic properties of graphenic nanostructures is instrumental in future spintronics applications. These magnetic properties are known to depend crucially on the presence of defects. Here we review our recent theoretical studies using density functional calculations on two types of defects in carbon nanostructures: substitutional doping with transition metals, and sp^3-type defects created by covalent functionalization with organic and inorganic molecules. We focus on such defects because they can be used to create and control magnetism in graphene-based materials. Our main results are summarized as follows:

1. Substitutional metal impurities are fully understood using a model based on the hybridization between the d states of the metal atom and the defect levels associated with an unreconstructed D_{3h} carbon vacancy. We identify three different regimes, associated with the occupation of distinct hybridization levels, which determine the magnetic properties obtained with this type of doping.

E.J.G. Santos (✉)
Centro de Física de Materiales (CFM-MPC) CSIC-UPV/EHU, Paseo Manuel de Lardizabal 5, San Sebastián 20018, Spain

Donostia International Physics Center (DIPC), Paseo Manuel de Lardizabal 4, San Sebastián 20018, Spain

Present address: Harvard School of Engineering and Applied Sciences, Harvard University, Cambridge, MA 02138, USA

Cruft Laboratory, Office Number: 406, 4th Floor, Oxford Street, Cambridge, MA 02138, USA
e-mail: esantos@seas.harvard.edu

A. Ayuela • D. Sánchez-Portal
Centro de Física de Materiales (CFM-MPC) CSIC-UPV/EHU, Paseo Manuel de Lardizabal 5, San Sebastián 20018, Spain

Donostia International Physics Center (DIPC), Paseo Manuel de Lardizabal 4, San Sebastián 20018, Spain
e-mail: swxayfea@ehu.es; sqbsapod@ehu.es

2. A spin moment of $1.0\,\mu_B$ is *always* induced by chemical functionalization when a molecule chemisorbs on a graphene layer via a single C–C (or other weakly polar) covalent bond. The magnetic coupling between adsorbates shows a key dependence on the sublattice adsorption site. This effect is similar to that of H adsorption, however, with universal character.
3. The spin moment of substitutional metal impurities can be controlled using strain. In particular, we show that although Ni substitutionals are nonmagnetic in flat and unstrained graphene, the magnetism of these defects can be activated by applying either uniaxial strain or curvature to the graphene layer.

All these results provide key information about formation and control of defect-induced magnetism in graphene and related materials.

2.1   Introduction

The experimental discovery of graphene, a truly two-dimensional crystal, has led to the rapid development of a very active line of research. Graphene is not only a fundamental model to study other types of carbon materials, but exhibits many uncommon electronic properties governed by a Dirac-like wave equation (Novoselov et al. 2004, 2005). Graphene, which exhibits ballistic electron transport on the submicrometer scale, is considered a key material for the next generation of carbon-based electronic devices (Geim and Novoselov 2007; Castro Neto et al. 2009). In particular, carbon-based materials are quite promising for spintronics and related applications due to their long spin relaxation and decoherence times owing to the spin-orbit interaction and the hyperfine interaction of the electron spins with the carbon nuclei, both negligible (Hueso et al. 2008; Trauzettel et al. 2007; Tombros et al. 2007; Yazyev 2008a). In addition, the possibility to control the magnetism of edge states in nanoribbons and nanotubes by applying external electric fields introduces an additional degree of freedom to control the spin transport (Son et al. 2006; Mananes et al. 2008). Nevertheless, for the design of realistic devices, the effect of defects and impurities has to be taken into account. Indeed, a substantial amount of work has been devoted to the study of defects and different types of impurities in these materials. The magnetic properties of point defects, like vacancies, adatoms, or substitutionals, have been recognized by many authors (Lehtinen et al. 2003; Palacios et al. 2008; Kumazaki and Hirashima 2008; Santos et al. 2010a,b; Chen et al. 2010; Ugeda et al. 2010; Yazyev and Helm 2007). It has now become clear that the presence of defects can affect the operation of graphene-based devices and can be used to tune their response.

In this chapter, we provide a review of several recent computational studies on the role of some particular type of defects in determining the electronic and, in particular, the magnetic properties of graphene and carbon nanotubes (Santos et al. 2008, 2010a,b, 2011, 2012a,b,c). We will consider two types of defects: substitutional transition metals and covalently bonded adsorbates. For the substitutional transition metals, we first present some of the existing experimental evidence about the

presence of such impurities in graphene and carbon nanotubes. Then, we summarize our results for the structural, electronic, and magnetic properties of substitutional-transition metal impurities in graphene. We show that all these properties can be explained using a simple model based on hybridization between the d shell of the metal atoms and the defects states of an unrelaxed carbon vacancy. We also show that it is possible to change the local spin moment of the substitutional impurities by applying mechanical deformations to the carbon layer. This effect is studied in detail in the case of Ni substitutionals. Although these impurities are nonmagnetic at a zero strain, we demonstrate that it is possible to switch on the magnetism of Ni-doped graphene either by applying uniaxial strain or curvature to the carbon layer. Subsequently, we explore the magnetic properties induced by covalent functionalization of graphene and carbon nanotubes. We find that the magnetic properties in this case are universal, in the sense that they are largely independent of the particular adsorbate: As far as the adsorbate is attached to the carbon layer through a single C–C covalent bond (or other weakly-polar covalent bond), there is always a spin moment of $1 \mu_B$ associated with each adsorbate. We show that this result can be understood in terms of a simple model based on the so-called π-vacancy, that is, one p_z orbital removed from a π-tight-binding description of graphene. This model captures the main features induced by the covalent functionalization and the physics behind. In particular, using this model, we can easily predict the total spin moment of the system when there are several molecules attached to the carbon layer simultaneously. Finally, we have also studied in detail the magnetic couplings between Co substitutional impurities in graphene. Surprisingly, the Co substitutional impurity is also well described in terms of a simple π-vacancy model.

2.2   Substitutional Transition-Metal Impurities in Graphene

2.2.1   Experimental Evidences

Direct experimental evidence of the existence of substitutional impurities in graphene, in which a single metal atom substitutes one or several carbon atoms in the layer, has been recently provided by Gan and coworkers (2008). Using high-resolution transmission electron microscopy (HRTEM), these authors could visualize individual Au and Pt atoms incorporated into a very thin graphitic layer probably consisting of one or two graphene layers. From the real-time evolution and temperature dependence of the dynamics, they obtained information about the diffusion of these atoms. Substantial diffusion barriers ($\sim 2.5\,\mathrm{eV}$) were observed for in-plane migration, which indicates the large stability of these defects and the presence of strong carbon–metal bonds. These observations indicate that the atoms occupy substitutional positions.